









RESEARCH ARTICLE | OCTOBER 24 2023

Cryo IR spectroscopy and cryo kinetics of dinitrogen activation and cleavage by small tantalum cluster cations

Daniela V. Fries ; Matthias P. Klein ; Annika Straßner ; Maximilian E. Huber ; Maximilian Luczak ; Christopher Wiehn ; Gereon Niedner-Schatteburg  



J. Chem. Phys. 159, 164303 (2023)

<https://doi.org/10.1063/5.0157217>

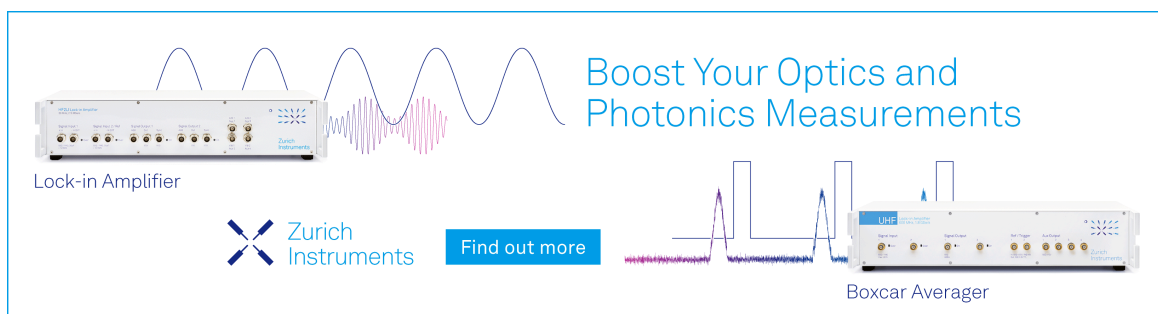


View
Online



Export
Citation

30 April 2024 06:34:47



Boost Your Optics and
Photonics Measurements

Lock-in Amplifier

Zurich
Instruments

Find out more

Boxcar Averager

Cryo IR spectroscopy and cryo kinetics of dinitrogen activation and cleavage by small tantalum cluster cations

Cite as: *J. Chem. Phys.* **159**, 164303 (2023); doi: [10.1063/5.0157217](https://doi.org/10.1063/5.0157217)

Submitted: 5 May 2023 • Accepted: 18 September 2023 •

Published Online: 24 October 2023










View Online



Export Citation



CrossMark

Daniela V. Fries,  Matthias P. Klein,  Annika Straßner,  Maximilian E. Huber,  Maximilian Luczak,  Christopher Wiehn,  and Gereon Niedner-Schatteburg 

AFFILIATIONS

Department of Chemistry and State Research Center OPTIMAS, Rheinland-Pfälzische Technische Universität (RPTU) Kaiserslautern-Landau, 67663 Kaiserslautern, Germany

^{a)} Author to whom correspondence should be addressed: gns@rptu.de

ABSTRACT

We investigate small tantalum clusters Ta_n^+ , $n = 2-4$, for their capability to cleave N_2 adsorption spontaneously. We utilize infrared photon dissociation (IR-PD) spectroscopy of isolated and size selected clusters under cryogenic conditions within a buffer gas filled ion trap, and we augment our experiments by quantum chemical simulations (at DFT level). All Ta_n^+ clusters, $n = 2-4$, seem to cleave N_2 efficiently. We confirm and extend a previous study under ambient conditions on Ta_2^+ cluster [Geng *et al.*, *Proc. Natl. Acad. Sci. U. S. A.* **115**, 11680–11687 (2018)]. Our cryo studies and the concomitant DFT simulations of the tantalum trimer Ta_3^+ suggest cleavage of the first and activation of the second and third N_2 molecule across surmountable barriers and along much-involved multidimensional reaction paths. We unravel the underlying reaction processes and the intermediates involved. The study of the N_2 adsorbate complexes of Ta_4^+ presented here extends our earlier study and previously published spectra from $(4,m)$, $m = 1-5$ [Fries *et al.*, *Phys. Chem. Chem. Phys.* **23**(19), 11345–11354 (2021)], up to $m = 12$. We confirm the priority published double activation and nitride formation, succeeded by single side-on N_2 coordination. Significant red shifts of IR-PD bands from these side-on coordinated μ_2 - $\kappa N:\kappa N,N$ N_2 ligands correlate with the degree of tilting towards the second coordinating Ta center. All subsequently attaching N_2 adsorbates onto Ta_4^+ coordinate in an end-on fashion, and we find clear evidence for co-existence of end-on coordination isomers. The study of stepwise N_2 adsorption revealed adsorption limits $m_{(max)}$ of $[Ta_n(N_2)_m]^+$ which increase with n , and kinetic fits revealed significant N_2 desorption rates upon higher N_2 loads. The enhanced absolute rate constants of the very first adsorbate steps $k_{(n,0)}^{abs}$ of the small Ta_3^+ and Ta_4^+ clusters independently suggest dissociative N_2 adsorption and likely N_2 cleavage into Ta nitrides.

© 2023 Author(s). All article content, except where otherwise noted, is licensed under a Creative Commons Attribution (CC BY) license (<http://creativecommons.org/licenses/by/4.0/>). <https://doi.org/10.1063/5.0157217>

INTRODUCTION

The natural nitrogen cycle consists of constant transformation of nitrogen between the earth's atmosphere, water, soils and biomass, and it is subject of anthropogenic interference that requires careful management strategies of the nitrogen budget.³⁻⁵ The industrial ammonia production from N_2 and H_2 is expensive in terms of energy consumption,⁶⁻⁸ yet irreplaceable, and at present it requires high amounts of fossil fuels as feedstocks. There are various protocols of NH_3 synthesis, and among them the Haber-Bosch process is most prominent.

It warrants to undertake knowledge driven research on the underlying processes which comprise the catalytic N_2 conversion, and much of the previous efforts in this regard have led to an award winning picture.⁹⁻¹¹ It is subject of ongoing research, and further optimization is mandatory.^{12,13} There are some comprehensive reviews that provide an overview of the current state of N_2 splitting reactions and follow-up nitrogen transfer reactivity proofs for a variety of transition metal (TM) and lanthanoid complexes.¹⁴⁻¹⁶ It was recognized that the N_2 coordination mode correlates with the propensity of N_2 functionalization, which in turn requires prior N_2 cleavage.¹⁷ An auspicious site for N_2 activation seem to originate

from isolated tantalum atoms on silica surfaces,¹⁸ and an N₂ side-on coordination seems critical.¹⁹

TM clusters receive ongoing attention as model systems for the study of elementary processes of catalytic relevance.^{20–22} Bare transition metal clusters of V, Gd and Sc are known to cleave N₂ spontaneously.^{23–25} Some homo- and hetero-metallic carbides were found to cleave N₂ and achieve C–N bond formation.^{26–29} Lithium doped TM complexes were also found to activate N₂.³⁰

Tantalum clusters are susceptible to oxide formation by O₂ and CO₂,^{31,32} and the stoichiometry of their oxides is known to affect N₂ uptake.³³ Similar effects and size dependencies arise in reactions with methane.^{34,35} Some prior studies on small tantalum clusters provide for evidence of dissociative N₂ adsorption. Geng *et al.* described the dinitride formation by Ta₂⁺ and Ta₂NN⁺ and elaborated crucial steps of the N₂ activation process by the tantalum dimer clusters.^{1,36} DFT modelling predicted N₂ cleavage by neutral and anionic trinuclear tantalum clusters,^{37,38} and there is further DFT modelling and some N₂ desorption experiments on small tantalum clusters, which supported conceivable N₂ cleavage.^{39,40}

While all of the above gained insights stem either from mass spectrometric experiments and/or quantum chemical modelling, it is an obvious need to provide additional spectroscopic characterization. A focus on cluster vibrations seems fertile. Inelastic electron scattering off N₂ layered Fe surfaces has proved valuable in this regard, and it helped to identify a characteristic 1555(30) cm⁻¹ feature as fingerprint of a likely precursor to N₂ dissociation while definite structural information remained sparse due to the limited spectral resolution.^{41,42} Infrared photon dissociation (IR-PD) spectroscopy may serve to complement, in particular when applied to isolated clusters and their complexes. Several studies utilized free electron lasers (FEL) and achieved similar or slightly better resolution.^{43–46} It is the table top sized Optical Parametric Oscillator (OPO) technology which augments FEL based research, and it enables the recording of sometimes better resolved spectra (± 5 cm⁻¹) of e.g. isolated cluster adsorbate complexes, and this method is widely applicable and well established much beyond TM cluster research by now.^{47–56} In any case it is the quantum mechanical modelling – appropriately conducted by DFT base methods – which takes the quest for explicit reaction path modelling of such gas phase reactions of isolated species, and for identification of participating intermediates, electronic states, barriers and crucial transition state geometries.^{21,57,58}

Experimental results from such IR-PD vibrational spectra of Ta_n⁺ clusters, n = 6–20, complemented by theoretical modelling provide for the geometries of these clusters, their relative stabilities and electronic properties.^{59,60} A 2022 perspective summarizes recent progress in the field of nitrogen activation by metal species in the gas phase, but also shows that a systematic understanding of cluster reactivity and N₂ activation and functionalization is lacking to date.⁶¹

Our current studies pick up this prevailing deficiency. We complement our prior study on Ta₄⁺² and thereby clarify the overall picture by a systematic study of N₂ on small tantalum clusters Ta_n⁺, n = 2–8. We have reacted these clusters with N₂ at 26 K and recorded IR-PD spectra of the adsorption species [Ta_n(N₂)_m]⁺, similar to our earlier studies on Ni, Rh, RhFe and Fe clusters.^{62–67}

In the present study [IRS1] we discuss the N₂ adsorption onto the three smallest cluster Ta_{2–4}⁺. In the adjoined IR-PD study [IRS2] we present findings for the N₂ adsorption onto the larger clusters Ta_{5–8}⁺. The findings of both studies, which we refer in the following as [IRS1] and [IRS2], respectively, find strong support through our complementary cryogenic kinetic study (cf. supplementary material). The combination of IR-PD measurements and DFT modeling with kinetic studies provides insights into the processes and structures involved in the adsorption, activation, and subsequent cleavage of the first few adsorbed N₂ molecules by Ta_{2–4}⁺. Furthermore, we gain insight into the coordination motifs and structures of the clusters with additional N₂ molecules, adsorbed on the small clusters after nitride formation.

EXPERIMENTAL AND COMPUTATIONAL METHODS

All experimental results presented were recorded using a customized Fourier transform ion cyclotron resonance (FT-ICR) mass spectrometer. (Apex Ultra, Bruker Daltonics). This FT-ICR instrument is used to generate cluster ions, select them by size, and coordinate them with N₂. The investigation of the respective cluster adsorption species is performed by mass spectrometry and infrared photon dissociation (IR-PD) spectroscopy. We refer to some of our previous publications for a detailed description of ion generation and N₂ adsorption process on TM clusters.^{2,62,63,67–70} Text S3 in the supplementary material also provides a comprehensive description, especially for Ta_n⁺ clusters. According to the routine described there, the ions are trapped in a RF hexapole ion trap and detected in the cryogenic (~10 K) FT-ICR trapping cell. In this ICR cell, the respective cluster adsorbates are irradiated with a tunable IR laser system (1200–2400 cm⁻¹, cf. Fig. S1 for a laser power curve). Absolute values of the DFM frequencies were derived from the online monitored OPO signal frequencies (continuous online wavemeter monitoring, *Bristol Instruments*, 8721B-NIR) and the pre-recorded value of the Nd:YAG frequency. A full description of the details of the laser system and its parameters can be found in the attached infrared spectroscopy study of Ta_{5–8}⁺ cluster [IRS2]. We record a series of fragmentation mass spectra during continuous scanning of the IR wavelength and evaluate the fragmentation efficiency of the measured IR-PD signals: frag. eff. = $\frac{\sum_i F_i}{\sum_i F_i + \sum_i P_i}$, F_i and P_i as fragment and parent ion signals. Finally, we obtain the IR-PD spectra for each species by plotting the fragmentation efficiencies as functions of the laser frequencies. For all irradiated species, N₂ loss was the only fragmentation channel observed.

We performed density functional modelling, geometry optimization and vibrational analysis using the program packages Gaussian 09⁷¹ and Gaussian 16 suite.⁷² The functional PBE0^{73,74} along with the Def2-TZVP basis set^{75,76} were applied for all atoms in (4,m) cases, and the Def2-TZVP basis set⁷⁵ for N atoms and cc-pVTZ-pp basis set⁷⁷ for Ta atoms in all (2,m) and (3,m) cases. We justify our choice of theory level by continuity with previous studies that have succeeded in predicting N₂ adsorption before^{64,67,69,70,78} – particularly for the adsorption, activation, and cleavage of N₂ on Ta₄⁺ clusters.² In all cases, we tolerated a relaxed SCF convergence criteria of 10⁻⁶ (as compared to 10⁻⁸ in “standard” DFT calculations) in order to achieve SCF convergence. All stationary points were checked for no and one imaginary frequency in cases of minima

and transition states, respectively. All conceivable isomers were optimized to stable minimum structures, and the most stable one was regarded as global minimum. Reaction paths were searched for by QST2/3^{79–81} and after location and optimization of the transition states calculated along the Intrinsic Reaction Coordinate (IRC).^{81,82} To better compare our results for the cleavage of N₂ on Ta₂⁺ with the results of Geng *et al.*¹ we also performed DFT modeling for the activation pathway with B3LYP hybrid functional,^{83,84} cf. Fig. S4. We applied a scaling factor of 0.9736 to the recorded IR-PD spectra of the cluster species (4,m), in order to account for the prevailing anharmonicities. Tables of unscaled IR-PD frequencies for all cases are documented in the supplementary material. Predicted and scaled IR frequencies were convoluted with gaussian profiles of fwhm = 5 cm⁻¹ in order to compare to the experimental IR-PD spectra.

DISCUSSION AND RESULTS

In addition to kinetic measurements [provided and discussed in the supplementary material (cf. Text S2 ff., Fig. S14 ff. and Table S26 ff.)], we extended our studies of N₂ adsorption on Ta_n⁺ clusters, n = 2–4, by IR-PD spectroscopy measurements of the N₂ adsorbates of these clusters under adiabatic conditions in the ion trap. Further IR-PD spectroscopy investigations of N₂ adsorption on Ta_n⁺ clusters, n = 5–8, can be found in our adjoined infrared study [IRS2].

We found a concise variation of recorded IR-PD features as a function of the Tantalum cluster size and of Nitrogen adsorbate loading. It is straightforward to assign these features to vibrational bands of the adsorbed N₂ chromophore. Frequent IR-PD features, in the majority of cases, locate in the range of 2000–2350 cm⁻¹. These features are fingerprinting N₂ moieties that correspond most likely to end-on adsorbates to single Tantalum centers with little to no interaction to other centers. This interpretation is in line with previously reported cases for Fe_n⁺,⁶⁷ Co_n⁺,⁶⁸ Ni_n⁺,^{62,63} Ru_n⁺,⁶⁹ Rh_n⁺⁷⁰ and even Ta₄⁺.² In several cases, we obtained IR-PD bands in the range of 1300–1700 cm⁻¹. In all cases but (4,3) these bands occur in addition to the afore mentioned ones.

The recorded IR-PD patterns distinguish by n, the Ta_n⁺ cluster size, in a remarkable way, and for a given n, they vary by m, the amount of N₂ adsorbate loading. We choose to organize the (n,m) matrix of IR-PD spectra in discussing these by given n per chapter one after the other.

[Ta₂(N₂)_m]⁺

First, we consider in detail the IR-PD spectrum of the smallest tantalum cluster adsorbate of the (n,m) matrix - the tantalum dimer species [Ta₂(N₂)₁]⁺: (2,1). In the range of 1900–2400 cm⁻¹ we observe no structured IR-PD signal (Fig. S2). This was to expect in view of previous DFT results which suggest swift activation of N₂ upon encounter to Ta₂⁺.¹ The resulting Ta–N stretching mode falls outside the available photon range of our current study. Nevertheless, we can confirm the claim that Ta₂⁺ adsorbs an N₂ molecule that is not terminally bound to the Ta₂⁺ dimer in an end-on coordination^{1,39} by noting the absence of experimental vibrational bands for (2,1) in the corresponding wavenumber range.

The work of Geng *et al.*¹ describes the initial formation of a “side-on/end-on binding mode” of the Ta₂⁺ N₂ complex as a

barrier-free process. Our own DFT modelling confirms an equivalent μ₂-κN:κN,N coordination for the cases of Ta₃⁺ (see later in this work) and Ta₄⁺ (previous work²). However, in all three cases of Ta₂⁺, Ta₃⁺ and Ta₄⁺, we find an initial N₂ end-on coordination and an additional barrier towards the μ₂-κN:κN,N motif (side-on/end-on binding mode). In the supplementary material (cf. Fig. S4) the reader finds a direct comparison of our results and those of Geng *et al.*, both conducted with the same DFT functional (B3LYP).

Both employed DFT functionals, PBE0 and B3LYP, predict a bare Ta₂⁺ dimer in a doubled state and somewhat less favorably in a quartet state. Both multiplicities provide for reaction pathways that run largely in parallel when computed by PBE0 (cf. Fig. 1), and with energy gaps of up to 30 kJ/mol at I_{2(2,1)} at the most. Some enhanced barriers at TS_{23(2,1)} and beyond in quartet states when computed at B3LYP level of theory (cf. Fig. S3). The predicted geometries (cf. Tables S2 and S4) of intermediates and barriers along the reaction path are comparable to those of Geng *et al.*¹ but for the missing entrance channel complex. In summary, a feasible and spontaneous N₂ bond cleavage by Ta₂⁺ seems well confirmed.

[Ta₃(N₂)_m]⁺

We recorded the IR-PD spectra of the tantalum trimer Ta₃⁺ with up to five N₂ adsorbate species, (3,m), throughout a wavenumber range of 1200–2400 cm⁻¹ (Fig. 2). The low yields of higher loaded adsorbate species (m > 5, cf. Fig. S21 in the supplementary material) hampered recording IR spectra of these.

The absence of any vibrational bands for the first three adsorbate complexes (3,1), (3,2) and (3,3) is striking. We have observed such behavior before, e.g. for the cases of (2,1), cf. above, and for (4,1) and (4,2).² It was explained by swift N₂ activation and cleavage after initial adsorption to the cluster surface. The case of (4,3) revealed a different behavior, and it seems to constitute a peculiar case: The third N₂ molecule initially adsorbs end-on to the tantalum tetramer and subsequently tilts into a coordination motif which is end-on and side-on across an edge of the tetramer (μ₂-κN1:κN1,N2). N₂ pre-activation gets stuck at this point and thereby provides for an IR fingerprint of this frozen intermediate, namely a highly red shifted NN stretching band at 1475 cm⁻¹. Thus, it seemed imperative to check for end-on and also for side-on coordination motifs in the cases of (3,m) species, and we chose the wavenumber range of our IR spectroscopic investigations accordingly. We found no evidence of a NN stretching vibrational band in the recorded IR spectra. This absence of NN stretching fingerprints hints towards a likely NN activation and a possible NN bond cleavage.

In contrast, the IR spectra of the species (3,4) and (3,5) reveal some broad vibrational bands in the range of 2100–2200 cm⁻¹ (Fig. 2). Nevertheless, it is obvious that the broad band of (3,4) comprises of several partially overlapping bands, likely three of them, peaking at about 2137, 2180, and 2204 cm⁻¹. When the above statement speculation of triple N₂ activation by Ta₃⁺ holds, it would be a single N₂ oscillator that causes the three observable bands in the recorded spectrum of (3,4). This finding might be taken as a strong indication for co-existing isomers, that might result from distinguishable Ta sites and their N nitrido load. Similarly, the IR spectrum of (3,5) reveals a clearly recognizable band pattern with a partially resolved sub structure. Besides the broad main band at 2146 cm⁻¹ there are two narrower side bands at 2173 and 2189 cm⁻¹.

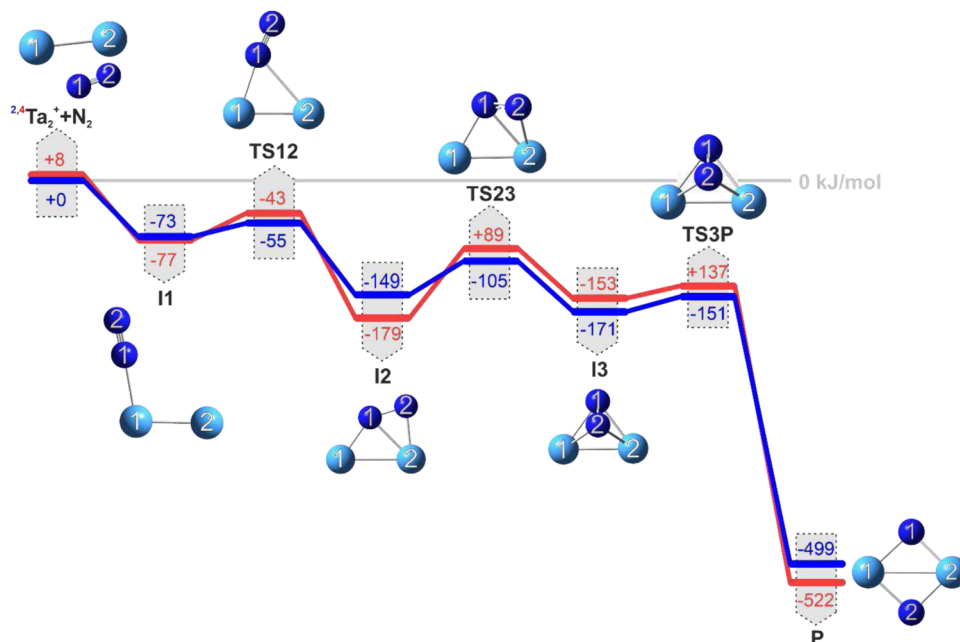


FIG. 1. Reaction pathway of N₂ cleavage by Ta₂⁺ (blue: doublet state, red: quartet state). Three submerged transition states allow for facile stepwise N₂ activation which ultimately leads to the dinitro product P_(2,1). Relative energies are in kJ/mol and displayed structures are those of doublet states with those of quartet states being very much comparable. For reason of clarity, the nomenclature is presented in an abbreviated form [e.g., I1 stands for I1_(2,1)].

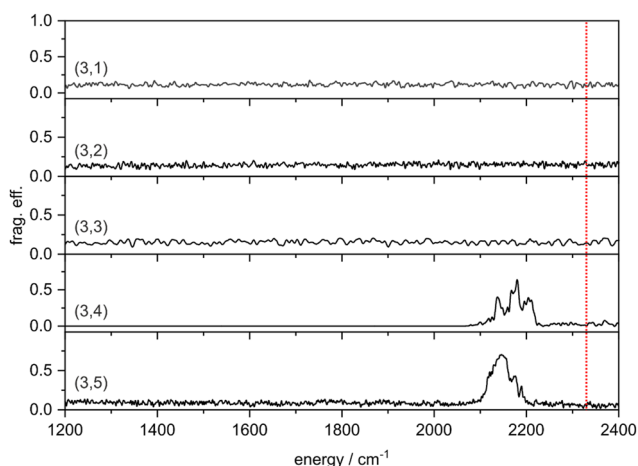


FIG. 2. IR spectra of Ta₃(N₂)_m⁺ [simplified nomenclature: (3,m)], m = 1–5 in the range of 1200–2400 cm⁻¹. Note the absence of vibrational bands in the cases of (3,1), (3,2) and (3,3). The bands in the cases (3,4) and (3,5) are significantly red shifted with respect to the free N₂ stretching vibrational frequency (2330 cm⁻¹,⁸⁵ red dotted line).

These three bands might indicate co-existing isomers as well. Due to the frequencies of the (3,4) and (3,5) bands, we assign them to N–N stretching vibrations of N₂ adsorbates which likely bind end-on to single tantalum centers – in line with previously reported cases of Fe_n⁺,⁶⁷ Co_n⁺,⁶⁸ Ni_n⁺,^{62,63} Rh_n⁺⁷⁰ and Ru_n⁺.⁶⁹ Furthermore, one

notices at first glance that the N₂ adsorbate bands for (3,4) and (3,5) are significantly redshifted with respect to the free N₂ stretching vibration frequency – –119.4 cm⁻¹ and –140.6 cm⁻¹, respectively – which would occur at 2330 cm⁻¹⁸⁵ (Fig. 2 red line). This shift is much in line with a sigma donor – pi acceptor synergistic model as stated before for CO adsorption to TM surfaces – the Blyholder model,⁸⁶ and as stated before for CO coordination in TM complexes – the Dewar Chatt Duncanson model.⁸⁷ We have adopted like explanations before, in the course of our previous investigations of N₂ adsorption to other transition metal clusters, e.g. of Fe_n⁺,⁶⁷ Co_n⁺,⁶⁸ Ni_n⁺,^{62,63} Rh_n⁺⁷⁰ and Ru_n⁺.⁶⁹

DFT modelling (3,0) → (3,1)

In order to obtain mechanistic insights into the N–N bond cleavage by the tantalum triangle we undertook systematic DFT modelling and obtained activation pathways in singlet, triplet and quintet state (Fig. 3, blue for quintet state, red for triplet state and green for singlet state). The naked Ta₃⁺ is high spin, quintet or triplet, and less stable by 59 kJ/mol in singlet. Molecular N₂ adsorption reduces this gap but keeps relative stabilities and yields 82–112 kJ/mol adsorption enthalpy by μ₁-κN1 end-on coordination of N₂, intermediate I1_(3,1) and perpendicular to the Ta₃⁺ triangle. The ²1_(3,1) intermediate on Ta₄⁺ assumes same angles but a longer Ta–N distance, d(Ta1–N1) = 2.13 Å in ²I1_(4,1) as compared to d(Ta1–N1) = 2.05/2.07/2.09 Å in ¹I1_(3,1)/³I1_(3,1)/⁵I1_(3,1). The interaction of molecularly adsorbed N₂ with Ta₃⁺ is thus somewhat more intimate than with Ta₄⁺, while spin state effects (such as high spin Pauli repulsion) are minor but discernible. In keeping with the prior

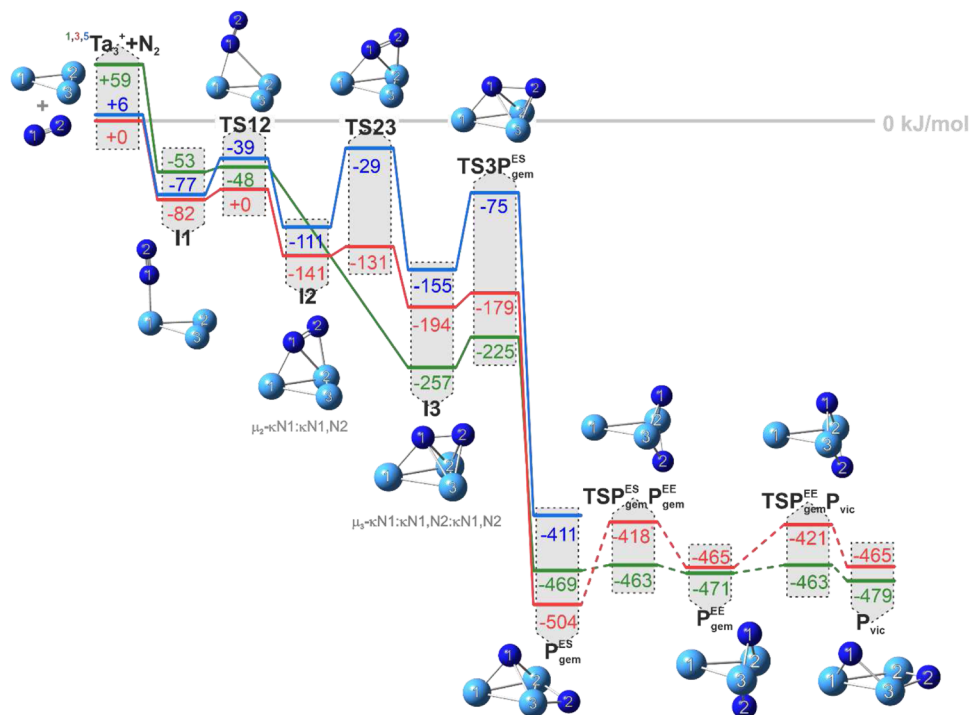


FIG. 3. Reaction pathways of N_2 cleavage by Ta_3^+ (green: singlet state, red: triplet state, blue: quintet state). Three submerged transition states allow for facile stepwise activation which ultimately leads to the dinitro product $P_{gem}^{ES(3,1)}$. Conversion via barriers into two more stable dinitro isomers $P_{gem}^{EE(3,1)}$ and $P_{vic}^{(3,1)}$ is possible. The subscript abbreviations *gem* and *vic* as well as ES and EE indicate geminal and vicinal as well as edge/surface and edge/edge coordination, respectively. Further details and the naming of these coordination motifs are more explicitly described in the supplementary material. Relative energies are in kJ/mol and geometry structures are triplet states. Note the torsional reorganization of the AEAS mechanism from an initial in-plane μ_2 - $\kappa N1:\kappa N1,N2$ coordination across an intact Ta–Ta edge towards perpendicular μ_3 - $\kappa N1:\kappa N1,N2:\kappa N1,N2$ coordination above the Ta–Ta–Ta surface. For reason of clarity, the nomenclature is presented in an abbreviated form [e.g. I1 stands for $I1_{(3,1)}$].

notation of $Ta_4^+ N_2$ adsorbate complexes we denote the $I1_{(3,1)}$ geometry of a sigma-bonded N_2 to a single Ta center as μ_1 - $\kappa N1$.

As soon as N_2 switches towards end-on μ_2 - $\kappa N1:\kappa N1$ coordination bridging two Ta centers, the high spin quintet state becomes less favorable, which is much in line with our previous observation of spin quenching by N_2 adsorption.^{64,67} For all of the remaining pathway of N_2 cleavage the high spin quintet state runs above and in parallel to the singlet and triplet state pathways which are more stable, and we omit it in further discussion. The switching step occurs through the nitrogen ligand tilting slightly towards the neighboring Ta2 atom across the transition state $TS12_{(3,1)}$. The low barrier towards ${}^3TS12_{(3,1)}$ is +11 kJ/mol, and the low barrier towards ${}^1TS12_{(3,1)}$ is +5 kJ/mol.

The singlet transition state ${}^1TS12_{(3,1)}$ invokes no reorganization of the Ta_3^+ triangle. The triplet transition state ${}^3TS12_{(3,1)}$ achieves its low barrier by significant elongation of the Ta1–Ta3 bond and concomitant shortening of the Ta2–Ta3 bond. As N1 moves in towards Ta2, Ta3 moves away from Ta1. In order to achieve the N_2 bridging configuration, the seeming “spectator” center Ta3 gives way and adopts. This works best in triplet configuration and it nicely illustrates the concept of induced fit among catalyst and substrate.

Beyond these transition states the further reaction pathways divert by spin state effects: The singlet state stabilizes directly towards the “above surface” intermediate ${}^1I3_{(3,1)}$, and there is no stable “across edge” intermediate by our DFT modelling. In contrast, the triplet state does stabilize into an “above surface” coordinated intermediate ${}^3I2_{(3,1)}$ by -70 kJ/mol, which is -59 kJ/mol below ${}^3I1_{(3,1)}$. This energetics come close to the corresponding ones of the Ta_4^+ case.² The bonding rearrangements are noteworthy: N_2 reorients from end-on coordination into a μ_2 - $\kappa N1:\kappa N1,N2$ asymmetric side-on coordination across a single edge of the Ta_3^+ triangle. This comes with an additional N2–Ta2 interaction that occurs while Ta3 comes back towards Ta1 by -0.05 Å. Thus, Ta3 acts almost like a directing gatekeeper, swinging forth (cf. above) and back.

The ${}^3I2_{(3,1)}$ intermediate manages to continue a reaction pathway with a reorganization from its μ_2 coordination (across edge) to a μ_3 coordination (above surface), which is labelled μ_3 - $\kappa N1:\kappa N1,N2:\kappa N1,N2$. This reorganization is the crucial step of the AEAS mechanism as observed in the case of Ta_4^+ before.² The barrier across ${}^3TS23_{(3,1)}$ is noticeably shallow (10 kJ/mol), in contrast to the according ${}^2TS23_{(4,1)}$ barrier (+58 kJ/mol). Above surface coordination in the ${}^3I3_{(3,1)}$ structure is favorable by -53 kJ/mol with respect to ${}^3I2_{(3,1)}$.

While spin coupling in naked Ta_3^+ favored high spin, the above surface coordination of the pre-activated N_2 adsorbate enforces spin quenching: $^1\text{I}_{3(3,1)}$ is more stable than $^3\text{I}_{3(3,1)}$ by -63 kJ/mol. Both N_2 bond lengths in $^1\text{I}_{3(3,1)}$ and $^3\text{I}_{3(3,1)}$, $d(\text{N1-N2}) = 1.36$ and 1.43 Å, respectively, exemplify another case of progressive N_2 activation, similar to $^2\text{I}_{3(4,1)}$, where N_2 has elongated to 1.43 Å as well.² The μ_3 coordinated N1 atom still experiences a C_3 symmetry breaking influence of its N_2 neighbor, which makes the opposite Ta1–N1 bond [$d(\text{Ta1-N2}) = 1.91$ Å] shorter by -0.24 Å than the Ta2–N1 and Ta3–N1 bonds [$d(\text{Ta2-N2}) = 2.15$ Å and $d(\text{Ta3-N2}) = 2.15$ Å].

Both $^1\text{I}_{3(3,1)}$ and $^3\text{I}_{3(3,1)}$ intermediates proceeds towards ultimate N_2 bond cleavage via $^{1/3}\text{TS3P}_{\text{gem}(3,1)}^{\text{ES}}$ across a barrier of $+32$ and $+15$ kJ/mol, respectively. At the transition states the N–N bond is further elongated by $+0.25$ to $+0.4$ Å with respect to the $\text{I}_{3(3,1)}$ states, and the N–N bond gets eventually lost towards the $\text{P}_{\text{gem}(3,1)}^{\text{ES}}$ product states, which is a remarkably exothermic process in all cases of spin states, -212 to -310 kJ/mol.

The nitride geometry of the favored $^3\text{P}_{\text{gem}(3,1)}^{\text{ES}}$ product state as displayed (Fig. 3) exemplifies singlet and quintet structures closely with some minor differences (cf. Tables S8–S11). It possesses a nitride atom each above the Ta triangle and across an edge (index ES for edge/surface). The μ_3 coordinated N1 atom shrinks its bond lengths towards all three Ta centers slightly by mere -0.05 Å with respect to $^3\text{I}_{3(3,1)}$. It however conserves its μ_3 coordination asymmetry of about -0.25 Å difference in Ta–N bond lengths as observed in $^3\text{I}_{3(3,1)}$. Thus, the C_3 symmetry breaking influence of N_2 is conserved even while it migrates around the Ta2–Ta3 axis, and while the pre-activated N1–N2 bond is cleaved.

In addition to the dinitro product $\text{P}_{\text{gem}(3,1)}^{\text{ES}}$ described above, we managed to identify two more stable $[\text{Ta}_3(\text{NN})]^+$ dinitro isomers: $\text{P}_{\text{gem}(3,1)}^{\text{EE}}$ and $\text{P}_{\text{vic}(3,1)}$. The former, $\text{P}_{\text{gem}(3,1)}^{\text{EE}}$, is characterized by the fact that the two N atoms locate across the same edge of the Ta3 triangle, the slightly elongated Ta2–Ta3 bond. Therefore, we denote this isomer with the indices *gem* (geminal, over the same edge) and *EE* (edge/edge). In the latter isomer, $\text{P}_{\text{vic}(3,1)}$, the two N atoms locate across two adjacent edges, denoted vicinal (*vic*). All three isomers have achieved full N–N bond cleavage. Each of the three product isomers, $\text{P}_{\text{gem}(3,1)}^{\text{ES}}$, $\text{P}_{\text{gem}(3,1)}^{\text{EE}}$ and $\text{P}_{\text{vic}(3,1)}$, provides for singlet and triplet states which are significantly lower than I_3 , but vary in relative stabilities: The singlet states of the three isomers are almost degenerate (± 10 kJ/mol) and they may easily convert into each other via low barriers ($+6$ to $+16$ kJ/mol). The triplet states behave differently: $^3\text{P}_{\text{gem}(3,1)}^{\text{EE}}$ and $^3\text{P}_{\text{vic}(3,1)}$ are less stable than $^3\text{P}_{\text{gem}(3,1)}^{\text{ES}}$, by about 39 kJ/mol, and the transition states come along with significant barriers of up to $+86$ kJ/mol. We therefore consider the most stable $^3\text{P}_{\text{gem}(3,1)}^{\text{ES}}$ as most likely product of the N_2 activation pathway.

In summary, the identified reaction path by our DFT modelling is overall declining (-504 kJ/mol) with all submerged barriers. Initial triplet and quintet states of Ta_3^+ seem to quench into the singlet $^1\text{I}_{3(3,1)}$ intermediate by N_2 coordination and exoergic activation, and the reaction proceeds towards ultimate N_2 cleavage via another spin flip, likely into most stable triplet state of geminal edge-surface N–N coordination. Most noteworthy, this Ta_3^+ activation pathway proceeds much in line with our previously identified across edge above surface (AEAS) mechanism of Ta_4^{+2} and shows similarities to the predicted N_2 cleavage at neutral an anionic $\text{Ta}_3^{0/+}$ clusters.^{37,38}

DFT modelling (3,1) → (3,2)

Previously, we found that Ta_4^+ manages to cleave subsequently two N_2 molecules as evidenced by the absence of IR fingerprint of coordinated and intact N_2 molecules for the first and the second Ta_4^+ adsorption species.² Here, we checked for a second NN triple bond cleavage by Ta_3^+ . The recorded IR spectra of $[\text{Ta}_3(\text{N}_2)_2]^+$ revealed no NN stretching bands between 1200 and 2400 cm^{-1} . This provides strong indication for a facile activation of a second N_2 molecule. In order to substantiate these findings we undertook DFT modelling, and we worked to find conceivable adsorption and activation pathways for a second N_2 molecule starting with the dinitro $\text{P}_{\text{gem}(3,1)}^{\text{ES}}$ as identified above (cf. Fig. 4). We consider singlet and triplet states and thus start with $^1\text{P}_{\text{gem}(3,1)}^{\text{ES}} + \text{N}_2$ and $^3\text{P}_{\text{gem}(3,1)}^{\text{ES}} + \text{N}_2$. All three Ta centers may act as coordination sides for a second N_2 adsorbate, Ta2 and Ta3 being equivalent due to C_s symmetry of $\text{P}_{\text{gem}(3,1)}^{\text{ES}}$. Thus, the DFT modelling yields four conceivable pathways for a second N_2 adsorption and activation: two singlet pathways, 1a and 1b, and two triplet pathways, 3a and 3b, each starting either through N_2 adsorption to Ta1 (pathways a) or to Ta3 (pathways b) (Fig. 4, dark green, light green, red, orange). Initial adsorption of the N_2 molecule yields intermediates $^{1a}\text{I}_{1(3,2)}$, $^{1b}\text{I}_{1(3,2)}$, $^{3a}\text{I}_{1(3,2)}$, or $^{3b}\text{I}_{1(3,2)}$ all of which possess the well-known end-on coordination of the N_2 either to Ta1 or to Ta3. The N_2 orients perpendicular to the Ta–Ta–Ta triangular facet at both sites. Among these four intermediates the triplet state of N_2 coordination to the Ta3 atom is most stable [$^{3b}\text{I}_{1(3,2)}$: -91 kJ/mol with respect to the triplet entrance channel].

As observed before in the cases first and second N_2 activation by Ta_4^+ , and in the present case of first N_2 activation by Ta_3^+ , the end-on bound N_2 ligand of the four $\text{I}_{1(3,2)}$ intermediate states bend towards the neighboring Ta atom via four transition states $\text{TS12}_{(3,2)}$ that comprise for barriers of $+27$ to $+73$ kJ/mol. These reorganizations eventually yield the $\text{I}_{2(3,2)}$ intermediates with the N_2 ligand coordinated in a μ_2 -κN3:κN3,N4 fashion, which is side-on across an edge of the Ta_3^+ cluster core, the Ta1–Ta3 bond. Note, that the two a pathways and the two b pathways encompass same kinetic motifs – the N_2 bending towards an across edge coordination – but in opposing directions: from Ta1 towards Ta3, pathways a, and vice versa from Ta3 towards Ta1, pathways b. Note furthermore, that singlet spin states become more stable than triplet states in $\text{I}_{2(3,2)}$, no matter which structure, a and b alike.

The next step of N_2 activation by the AEAS mechanism would involve a reorganization of the N_2 ligand from the μ_2 -κN3:κN3,N4 side-on coordination across an Ta–Ta edge in $\text{I}_{2(3,2)}$ towards a μ_3 -κN3:κN3,N4:κN3,N4 above surface coordination. By and large, this is what our DFT modeling yields in the present case, once more.

Along the b pathways, the reorganizations from $^{1b}\text{I}_{2(3,2)}$ and $^{3b}\text{I}_{2(3,2)}$ proceed via unfavorable $^{1b}\text{TS23}_{(3,2)}$ ($+122$ kJ/mol) and $^{3b}\text{TS23}_{(3,2)}$ ($+70$ kJ/mol) directly into $^{1b}\text{I}_{3(3,2)}$ and $^{3b}\text{I}_{3(3,2)}$. The high barriers seem to originate from N–N repulsion among N3 (of second N_2) and N2 (of first N_2). Subsequent N4 movement into final μ_2 coordination in I_3 seems facile, and it proceeds directly. N4 is not hindered by N1, and there is no further intermediate involved.

Instead, the pathways involve additional intermediates $^{1a}\text{I}_{23(3,2)}$ and $^{3a}\text{I}_{23(3,2)}$ connecting the respectively $^a\text{I}_{2(3,2)}$ and $^a\text{I}_{3(3,2)}$ states via consecutive transition states $^a\text{TS223}_{(3,2)}$ and $^a\text{TS233}_{(3,2)}$. The

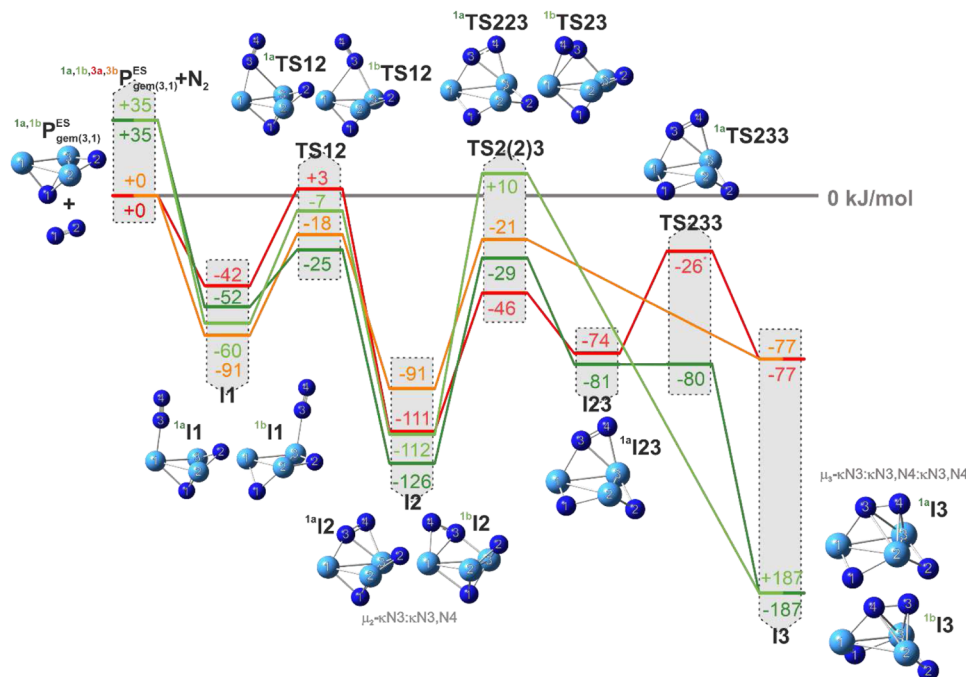


FIG. 4. Reaction pathways of a second N₂ activation by the dinitro species P^{ES}_{gem(3,1)}; two singlet pathways, 1a (dark green) and 1b (light green), and two triplet pathways, 3a (red) and 3b (orange), each of them starting either through N₂ adsorption to Ta1 (paths a) or to Ta3 (paths b). There is a striking similarity to the first cleavage pathway cf. Fig. 3: reorganization of the in-plane μ₂-κN3:κN3,N4 coordination across an intact Ta-Ta edge towards perpendicular μ₃-κN3:κN3,N4:κN3,N4 coordination above the Ta-Ta-Ta surface. Starting from the most likely product complex P^{ES}_{gem(3,1)} of the activation pathway of the first N₂ molecule by Ta₃⁺ the pathway for a second N₂ molecule activation yields in the intermediate I_{3(3,2)} which is independent of initial N₂ coordination to the Ta1 (paths a) or Ta3 (paths b) atom and gets stuck in front of unsurmountable barriers that hamper any further or ultimate NN bond cleavage (cf. Fig S5). For reason of clarity, the nomenclature is presented in an abbreviated form [e.g. I1 stands for I_{1(3,2)}].

^aTS223_(3,2) transition states are more stable than the ^bTS23_(3,2) of b pathways. ^aTS223_(3,2) does not suffer N-N repulsion, as both nitrido atoms N1 and N2 (originating from the first N₂ adsorbate) locate below the Ta₃ plane. However, N₂ needs to wag around the Ta₂-Ta₃ bond and further below the Ta₃ plane in order to allow for N₄ to locate above the Ta₂-Ta₃ edge. This N₂ downwards wagging becomes possible through concerted N1 upwards wagging around the Ta₁-Ta₂ bond, and it brings the cluster complex into ^{1a}I23 or ^{3a}I23. Spin state seems of little importance up to here. In contrast, the barriers towards ^{1a}I3_(3,2) or ^{3a}I3_(3,2) vary by spin states, with some uncertainty remaining. The influence of spin coupling increases significantly towards the next intermediate I3_(3,2).

The reorganization from I2_(3,2) to I3_(3,2) occurs in concerted manner way via the b pathway (a single TS) or in a consecutive manner via the a pathway (two TSs).

At this point, the modelled activation pathways yield in the intermediate I3_(3,2) which is independent of initial N₂ coordination to the Ta1 (paths a) or Ta3 (paths b) atom. I3_(3,2) comprises of an μ₃-κN3:κN3,N4:κN3,N4 above surface coordination of the second N₂ adsorbate with an enlarged N3-N4 bond length of d(N3-N3) = 1.36 Å.

Note, that the two N atoms of the fully activated first N₂ adsorbate, N1 and N2, underwent reorganization from prior edge/surface

(ES) coordination in P^{ES}_{gem(3,1)} into an edge/edge (EE) motif in I3_(3,2). It seems as if the N atom which was coordinated above the Ta-Ta-Ta triangle surface had to finally give way for the I3 above surface coordination of the second N₂ ligand.

Most notably, the singlet triplet splitting becomes of importance in I3_(3,2). It rises up to 110 kJ/mol in favor of singlet ¹I3_(3,2), which is three times higher than at the starting point P^{ES}_{gem(3,1)} + N₂. N₂ adsorbate induced spin quenching sets in at this point, much in line with what was observed by us in some cases before.^{64,67}

At this point further activation of the second N₂ molecule in [Ta₃(NN)(N₂)₁]⁺ would proceed in principle from singlet ¹I3_(3,2), -187 kJ/mol beneath the entrance channel, while the triplet ³I3_(3,2) is not populated. However, any found pathway towards ultimate N₂ bond cleavage would imply to surmount significant barriers [+154 kJ/mol, +190 kJ/mol or +221 kJ/mol above ¹I3_(3,2)], cf. Fig S5 in the supplementary material, which we consider unlikely. The adsorption and activation pathways seem to get stuck at ¹I3_(3,2) in front of these barriers which have unsurmountable under isothermal conditions.

Reviving the absence of N₂ fingerprints between 1200 and 2400 cm⁻¹ in the experimental IR spectrum of the [Ta₃(N₂)₂]⁺ adsorbate species, for which we therefore expect a complete cleaved NN bond even for the second N₂ molecule by Ta₃⁺, it is a urgent

need to check the calculated IR frequency of the $I_{3(3,2)}$ above surface coordination of the second N_2 ligand. And indeed, DFT calculations revealed a frequency at 1093 cm^{-1} for the respective NN stretching mode. Thus, the enlargement of the NN bond to 1.36 \AA is sufficient to shift the NN stretching mode outside our currently accessible spectral range of measurements.

In summary we can conclude at this point that successful and facile cleavage of a first N_2 molecule by Ta_3^+ is followed by the second N_2 molecule proceeding via similar activation steps: from initial end-on coordination through a second intermediate, with a $\mu_2\text{-}\kappa N_3:\kappa N_3,N_4$ bonded N_2 across an edge of the Ta_3^+ triangle core towards a $\mu_3\text{-}\kappa N_3:\kappa N_3,N_4:\kappa N_3,N_4$ bonded N_2 ligand at intermediate $I_{3(3,2)}$. The cluster complex seem to get stuck in $I_{3(3,2)}$ in front of barriers that hamper further activation ($N_3\text{-}N_4$ bond enlargement beyond 1.36 \AA) under isothermal conditions. Whether ultimate NN bond cleavage into P_{gem} products (Fig. S5) does take place, depends on the experimental conditions. Verification would be subject of further spectroscopic verification, e.g. by the recording of TaN nitride fingerprint patterns through far IR radiation exposure by a free electron laser.

DFT modelling (3,2) \rightarrow (3,3)

We checked for feasible adsorption pathways of a third N_2 molecule to the Ta_3^+ cluster, and we started with singlet $I_{3(3,2)}$, a likely product of the second N_2 adsorption (cf. Fig. 5). The $I_{3(3,2)}$ structure provides for two preferential N_2 coordination sites, Ta1 and Ta3, the Ta2 suffering from steric hindrance. Thus, we conceive two distinguishable coordination motifs for initial end-on N_2 adsorption: $^{1a}I_{1(3,3)}$ for N_2 adsorption to Ta1 (Fig. 5, dark green pathway) and $^{1b}I_{1(3,3)}$ for N_2 adsorption to Ta3 (Fig. 5, light green pathway), both intermediates being almost degenerate.

Subsequent tilting towards the neighboring Ta cluster core atom proceeds via $^{1a}TS_{12(3,3)}$ and $^{1b}TS_{12(3,3)}$ with barriers just below the entrance channel (-3 and -4 kJ/mol) and yield $^{1a}I_{2(3,3)}$ and $^{1b}I_{2(3,3)}$, respectively. As coordination motif of the $I_{2(3,3)}$ intermediates we found the N_2 ligand to be coordinated in a $\mu_2\text{-}\kappa N_5:\kappa N_5,N_6$ fashion, which is side-on across an edge of the Ta_3^+ cluster core, the Ta1–Ta3 bond. Note, that the a pathway and the b pathway encompass same kinetic motifs – the N_2 bending towards an across edge coordination – but in opposing directions: from Ta1 towards Ta3, pathways a, and vice versa from Ta3 towards Ta1, pathways b. Although both $I_{2(3,3)}$ intermediates are $+19\text{ kJ/mol}$ or rather $+13\text{ kJ/mol}$ less stable than the respective $I_{1(3,3)}$ intermediates both are [$^{1a}I_{2(3,3)}$: -35 kJ/mol , $^{1b}I_{2(3,3)}$: -42 kJ/mol] significantly more stable than the entrance channel.

A consecutive step of N_2 activation by the AEAS mechanism would involve a reorganization of the N_2 ligand from the $\mu_2\text{-}\kappa N_5:\kappa N_5,N_6$ side-on coordination across an Ta–Ta edge in $I_{2(3,2)}$ towards a $\mu_3\text{-}\kappa N_5:\kappa N_5,N_6:\kappa N_5,N_6$ above surface coordination. However, the Ta_3^+ cluster core is quite highly loaded from the two prior N_2 adsorptions at this point, and another μ_3 above surface coordination seems unlikely. Instead we managed to find a feasible reorganization, via transition states $^{1a}TS_{2III(3,3)}$ and $^{1b}TS_{2III(3,3)}$, from the $I_2\ \mu_2\text{-}\kappa N_5:\kappa N_5,N_6$ single side-on N_2 motif into a $\mu_2\text{-}\kappa N_5,N_6:\kappa N_5,N_6$ double side-on “butterfly” N_2 motif across the Ta1–Ta3 edge, yielding a single $^{1a,1b}III_{(3,3)}$ intermediate, as identified in (2,1) before.¹

In the present (3,3) case, the intermediate $^{1a,1b}III_{(3,3)}$ is $+38\text{ kJ/mol}$ less stable than the entrance channel. Further reorganization into an about -18 kJ/mol more stable cluster adsorbate species $IV_{(3,3)}$ would require to surmount a barrier of $+180\text{ kJ/mol}$ ($TS_{III\ IV(3,3)}$), which seems unlikely.

At this point we like to correlate this predicted reaction path to our experimental IR spectroscopic findings. We aim to identify the actually populated product, and we take the intermediates $^{1a}I_{1(3,3)}$ and $^{1b}I_{1(3,3)}$ or $^{1a}I_{2(3,3)}$ and $^{1b}I_{2(3,3)}$ as well as $^{1a,1b}III_{(3,3)}$ into account. The $^{1a}I_{1(3,3)}$ and $^{1b}I_{1(3,3)}$ intermediates should provide for recordable IR fingerprints of end-on NN stretching vibration in the range of $2000\text{--}2400\text{ cm}^{-1}$.^{2,62,63,67–70} The absence of such fingerprints in our recorded (3,3) IR spectrum discards these intermediates. Predicted IR frequencies of tilted N_2 stretching vibration in $^{1a}I_{2(3,3)}$ and $^{1b}I_{2(3,3)}$ are 1816 and 1764 cm^{-1} , respectively (unscaled values). No according IR signals recorded we abandon these intermediates as well. The remaining $III_{(3,3)}$ intermediate provides for predicted NN stretching frequencies below 1144 cm^{-1} (unscaled), which is in line with our observations.

So far DFT calculations are in line with our IR measurements. However, we have to address explicitly the fact that the intermediate $III_{(3,3)}$ is $+38\text{ kJ/mol}$ less stable than the entrance channel. At this point it seems helpful to consider the big picture of consecutive N_2 adsorption to Ta_3^+ (cf. Fig. 6): The tantalum trimer manages to cleave the first adsorbed N_2 molecule (cf. Fig. 3, reaction path by DFT) and the subsequent adsorption of a second N_2 likely starts at $^3P_{\text{gem}}^{ES(3,1)}$, and it yields $I_{3(3,2)}$ (see Fig. 4, reaction path by DFT). By these two highly exothermic adsorption events, this $I_{3(3,2)}$ adsorption complex has stabilized by more than 600 kJ/mol . While the He buffer gas is certainly able to thermalize the stored ionic complex on the long run, it certainly takes a multitude of He collisions to achieve full thermalization. Thus, it is likely that $I_{3(3,2)}$ possess some internal energy when subsequently encountering a further N_2 partner. Thereby it becomes possible to explore the (3,3) potential hypersurface along a direct reaction up to $^{1a,1b}III_{(3,3)}$ (cf. Fig. 5, reaction path by DFT) where it might get stuck in front of a seemingly unsurmountable barrier. Of course, it is conceivable to invoke the alternative possibility of a third N_2 addition and reaction to a fully activated $Ta_3N_4^+$ moiety in P_{gem} configuration (Fig. S5). DFT modelling and far IR spectral verification would be subject of future works.

Our further DFT modelling suggests swift adsorption of the fourth N_2 partner without further barriers and into some stable N_2 end-on coordination. It seems likely that $^{1a,1b}III_{(3,3)}$ sustains its priorly achieved structural motifs: an I_3 above surface coordination motif, one double-bridged triangular edge and two one single-bridged triangular edge. In effect, the additional end-on coordinating N_2 ligand may assume any of three available adsorption sites, Ta1, Ta2 or Ta3. These differ in the number of nearest neighbors. Geometry optimization of the singlet states of these resulting three isomers yield almost degenerate states $^1(3,4)^{Ta1}$, $+8\text{ kJ/mol}$, $^1(3,4)^{Ta2}$, and $^1(3,4)^{Ta3}$, $+6\text{ kJ/mol}$. Accordingly we expect all three isomers likely populated, and three slightly different IR active NN stretching frequencies. Indeed, the (3,4) IR-PD spectrum comprises of three partially resolved bands which strongly support the likely presence of end-on coordinated N_2 ligands in any of three different coordination sites. The DFT modelling provides for predictions on the harmonic frequencies of the N_2 stretching vibrations at

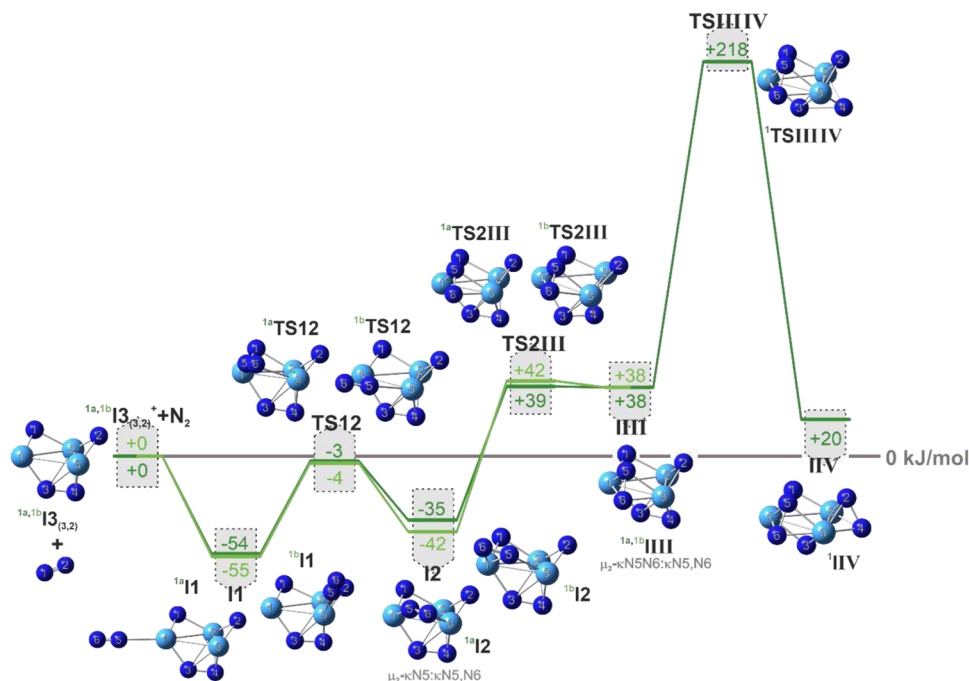


FIG. 5. Reaction pathways of a third N_2 adsorption by the dinitro species $I3_{(3,2)}$: two singlet pathways, 1a (dark green) and 1b (light green) starting either through N_2 adsorption to Ta1 (pathway a) or to Ta3 (pathway b). For the first steps of the pathway there is a striking similarity to the first and second N_2 activation pathways cf. Figs. 3 and 4: initial end-on adsorption of the N_2 ligand and subsequent tilting of the N_2 towards a neighboring Ta atom, eventually yielding an in-plane μ_2 - $\kappa N3:\kappa N3,N4$ coordination across an intact Ta–Ta edge. Starting from the most likely product complex ${}^1I3_{(3,2)}$ of the activation pathway of the second N_2 molecule by $Ta3^+$ the adsorption pathway for a third N_2 molecule yields the intermediate $III_{(3,2)}$ which is independent of initial N_2 coordination to the Ta1 (path a) or Ta3 (path b) atom and gets stuck in front of unsurmountable barriers that hamper any further or ultimate NN bond cleavage. For reason of clarity, the nomenclature is presented in an abbreviated form [e.g. I1 stands for $I1_{(3,3)}$].

these three sites, and they agree qualitatively. Due to large ambiguities in the applicable anharmonic scaling factors, it is not possible to achieve a quantitative comparison, however (cf. Table S19 and Fig. S6 in the supplementary material).

Accordingly, we recorded an experimental IR spectrum of the (3,5) cluster adsorbate complex. Besides the main band at 2146 cm^{-1} it reveals two side bands at 2173 and 2189 cm^{-1} . These hint towards distinguishable isomers once more. We managed to determine at least two likely structures by DFT calculations, ${}^1(3,5)^{Ta2,Ta3}$ and ${}^1(3,5)^{Ta1,Ta2}$ (see Table S20 and Fig. S6). Both structures reveal a strong IR active vibration, and a weak one, which are split by $40\text{--}50\text{ cm}^{-1}$. While absolute frequencies suffer from the before mentioned ambiguity of scaling factors, the predicted splitting are much less affected, and they agree well with the observed ones. We therefore consider a mixture of the two singlet minimum structures as a likely explanation for the observed IR bands of (3,5).

As the fourth and fifth N_2 molecule adsorb to merely two out of three possible coordination sites there is one coordination site vacant for adsorption of a sixth N_2 molecule filling up the second adsorption shell of N_2 on the $Ta3^+$ cluster for (3,6). We failed to obtain an IR spectrum of (3,6) due to its low abundance.

At this point, we want to address the question, whether the DFT predictions and the recorded IR-PD spectra are in line with the recorded adsorption kinetics (cf. Text S8, Fig. S21–S23 and Tables S29 and S30 in the supplementary material). These kinetics reveal

equally fast adsorption of first, second, fourth, and fifth N_2 molecule. The adsorption of the third and sixth N_2 molecule occur discernably slower, and the desorption is facile as evidenced by high values of $k_{(3,3)}$ and $k_{(3,6)}$. This indicates a likely meta stability of the formed $(3,3)^*$ and $(3,6)^*$ complexes. While the interpretation of the latter case would be much involved, the prior case of three N_2 adsorbates is well in line with the DFT predictions: It swiftly forms from a “hot” precursor $I3_{(3,2)}$, and it likely converts much of its stabilization into internal excitation. Note, that the larger the complexes, which involves increasing amounts of N_2 adsorbates, the swifter thermal relaxation and collisional cooling proceeds, and the larger the density of states becomes. Thus, the subsequent formation of larger complexes seems much less hampered by internal excitation.

$[Ta_4(N_2)_m]^+$

We extended the published spectra of $(4,m)$, $m = 1\text{--}5$,² by the present work up to $m = 12$ (Fig. 7). In short, the published spectra have revealed the following: The first two adsorbed N_2 molecules undergo unconditional cleavage and yield TaN motifs. A single IR-PD band at 1475 cm^{-1} of the (4,3) spectrum was assigned to a side-on (above edge, μ_2 - $\kappa N:\kappa N,N$) activated N_2 intermediate.² In addition, there is a very broad unstructured IR-PD signal above 1500 cm^{-1} , up to 2400 cm^{-1} , and likely further beyond, which might originate from a low lying electronic absorption of (4,3) to (4,5)

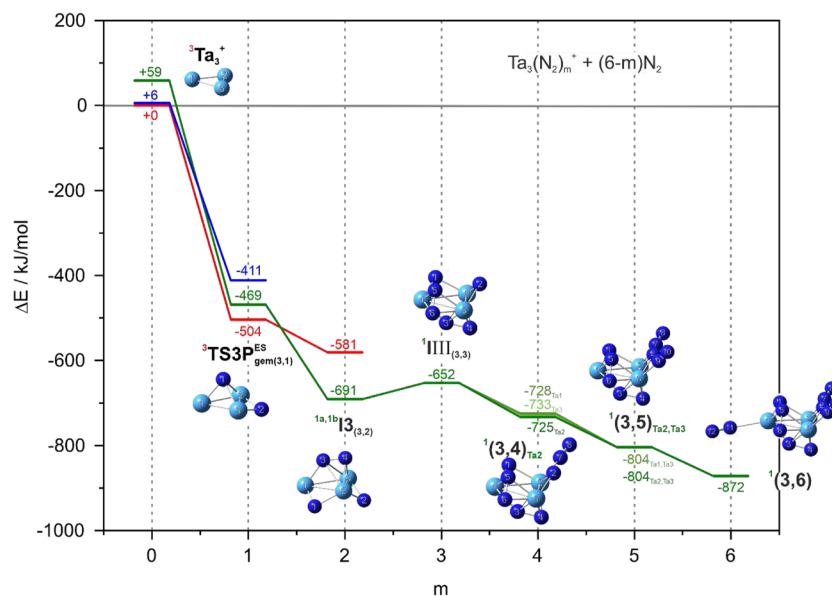


FIG. 6. The big picture of consecutive N_2 adsorption to Ta_3^+ . Ta_3^+ manages to cleave the first adsorbed N_2 molecule (cf. Fig. 3), and the subsequent adsorption of a second N_2 likely starts at ${}^3PES_{gem(3,1)}$, and it yields ${}^1I_{3(3,2)}$ (see Fig. 4). By these two highly exothermic adsorption events, this ${}^1I_{3(3,2)}$ adsorption complex has stabilized by more than 600 kJ/mol. It is likely that ${}^1I_{3(3,2)}$ possess some residual internal energy when subsequently encountering a further N_2 partner. Thereby it becomes possible to explore the (3,3) potential hypersurface along a direct reaction up to ${}^1III_{(3,3)}$ (cf. Fig. 5) where it finally gets stuck in front of a seemingly unsurmountable barrier.

complexes. The additional absorption around 2200–2300 cm^{-1} may arise from an end-on loosely bound N_2 molecule, which populates several isomers.

The newly recorded IR-PD spectra of the present work reveal the following: The IR-PD spectrum of the (4,6) cluster adsorbate complex displays a strong band at 1424 cm^{-1} , together with a medium strong sideband at 1435 cm^{-1} . Both likely indicate side-on μ_2 - $\kappa N:\kappa N,N$ N_2 adsorption. Two very weak absorptions occur at 1489 and 1580 cm^{-1} . In general, we assign all bands below 2000 cm^{-1} to side-on μ_2 - $\kappa N:\kappa N,N$ adsorbed N_2 molecules, and we take a variation of band position as indicators for varying motifs in the particular adsorption geometries. In the range of end-on coordinated N_2 adsorbates, above 2000 cm^{-1} , we find a strong band at 2252 cm^{-1} and four medium strong, sharp bands at 2209, 2224, and 2294 cm^{-1} . Note, that these bands are red shifted with respect to the free N_2 stretching vibration at 2330 cm^{-1} ⁸⁵ which is understood in terms of a σ -donor π -acceptor synergism that softens the N–N bond. This concept has been utilized for CO adsorbates in the Blyholder model⁸⁶ and for N_2 adsorbates in our earlier studies on Co_n^+ , Ni_n^+ , Fe_n^+ , Ru_n^+ , Rh_n^+ , and Rh_iFe_j alloy clusters.^{62,63,67–70,88,89} In the light of these findings, it is most noteworthy that we find another sharp IR-PD band at 2334 cm^{-1} which almost coincides with the free N_2 stretching vibration. This indicates that the corresponding N_2 molecule is very weakly bound to the cluster and therefore resemble an almost free, likely roaming N_2 molecule. Note, that any minute symmetry breaking of side-on N_2 coordination suffices to induce a non-vanishing dipole moment derivative. Thus, a “roaming” or second shell N_2 adsorbate may well acquire some IR transition moment.

The IR-PD spectrum of (4,7) resembles largely that one of (4,6), but with less bands in both regions of the spectrum: In the side-on N_2 range of the IR-PD spectrum, there is one strong (below 2000 cm^{-1}), sharp band at 1422 cm^{-1} and two weak bands at 1478 and 1535 cm^{-1} . In the end-on N_2 range above 2000 cm^{-1} , a sharp band at 2284 cm^{-1} appears, accompanied by a weak band at 2249 cm^{-1} . Finally, the 2333 cm^{-1} band much resembles an almost free N_2 as in (4,6). Such a band appears in all following (4,m) IR-PD spectra up to the largest observable cluster adsorbate complex (4,m(max)) $\hat{=}$ (4,12). It is most remarkable that a high loading of an odd number of N_2 molecules – namely seven – on a cluster of merely four Ta atoms provides for solely two sharp main bands – one in the side-on and one in the end-on N_2 range. Such a low amount of IR-PD bands from a high number of ligands indicates a very high symmetrical arrangement of the N_2 ligands within the cluster adsorption complex (4,7). Considering the findings from our prior study on the adsorption, activation and cleavage of the first few N_2 molecules on the Ta_4^+ cluster, it seems most likely that the species (4,7) possesses two cleaved and at least one activated N_2 ligand. This looks highly asymmetric.² The four subsequent N_2 molecules which yield (4,7) are most likely end-on bound N_2 ligands. It is somewhat surprising that the resulting quite simple IR-PD spectrum indicates high symmetry.

In noticeable contrast to the merely two sharp main bands for species (4,7) we observe a larger total amount of bands in the IR-PD spectrum of (4,8). There are three sharp and intensive bands in the side-on range: at 1413, 1468, and 1564 cm^{-1} . The former is accompanied by two weak sidebands, one to the right (1431 cm^{-1}) and one on the left (1394 cm^{-1}). In the end-on range of the spectrum,

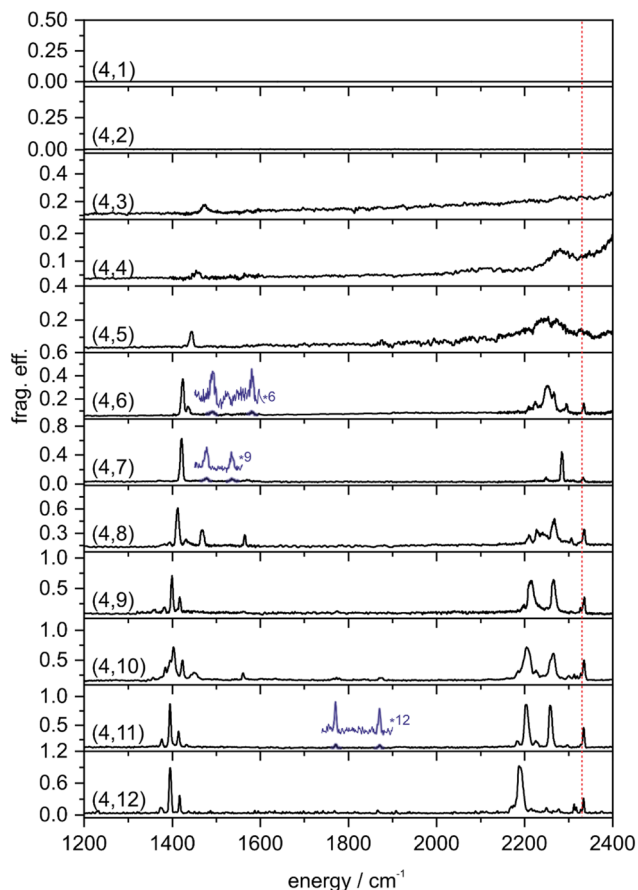


FIG. 7. IR-PD spectra of sequential N_2 adsorption steps onto Ta_4^+ cluster cations $[Ta_4(N_2)_m]^+$, $m = 1-12$, as recorded after 26 K He buffer gas cooling. The (4,1) to (4,5) spectra have been published before (Ref. 2, Fig. 2 therein). Note the significant red-shift of the IR-PD bands with respect to the free N_2 stretching vibrational frequency (2330 cm^{-1} ,⁸⁵ red dotted line).

we observe a broad absorption pattern with maxima at 2210, 2227, 2241, 2268, 2292, 2306, and 2335 cm^{-1} . The amount of 11 absorption maxima exceeds the number of eight N_2 oscillators and likely arises from co-existing isomers. A formal double N_2 occupation of some Ta atoms may combine with reorganization and isomerization. Note, that the enhanced width ($\sim 15\text{ cm}^{-1}$) of the strongest end-on band (2268 cm^{-1}) points towards a lack of high symmetry.

Some of the (4,9) bands coincide with those of (4,8). One notices the sharp and intense band at 1399 cm^{-1} with its both sidebands on the right (1383 cm^{-1}) and left side (1417 cm^{-1}). Very weak absorptions appear at 1361 and 1561 cm^{-1} . The three remaining main bands in the end-on range shift only slightly with respect to matching ones in (4,8): they appear at 2216 , 2265 , and 2336 cm^{-1} . The latter one shows a weak sideband to the left at 2327 cm^{-1} both of which match the free N_2 vibration quite well. This indicates that in species (4,9) likely two N_2 ligands are very weakly bound to the cluster core.

The general band pattern of (4,9) continues upon addition of further N_2 molecules up to (4,11). Total IR-PD yields of (4,10) are

high, and most of the numerous recorded bands are quite strong, yet still sharp, in part. We recognize absorption maxima at 1384 , 1403 cm^{-1} (with an indication of a sideband at 1395 cm^{-1} to the left), 1423 , and 1449 cm^{-1} . A band at 1561 cm^{-1} is also strikingly clear and intense. A similar band was already evident in the IR-PD spectrum of the species (4,8). All in all, the IR-PD band in the lower range appear somewhat broader than those of the (4,9) complex. In the end-on N_2 range we observe three intensive IR-PD bands at 2204 , 2265 , and 2335 cm^{-1} . The former is accompanied by two weak sidebands, one to the right (2226 cm^{-1}) and one to the left (2185 cm^{-1}), and the latter by a weak sideband at 2328 cm^{-1} . We also recognize three weak IR-PD adsorption bands at 2300 , 2313 and 2319 cm^{-1} .

It may be worthwhile to mention in passing that at this point the recorded IR-PD spectrum of (4,11) “simplifies” in terms of the total number of observed bands (ten) as compared to the IR-PD spectrum of (4,10) which provides for significantly larger number of IR-PD bands in total, namely 16. The bands of (4,11) resemble the (4,9) spectrum almost perfectly. The bands at 1376 , 1395 , 1414 , 2183 , 2202 , 2225 , 2258 , 2283 , 2297 , and 2334 cm^{-1} are only slightly red shifted with respect to those of (4,9), by up to 14 cm^{-1} and somewhat better separated. The good quality of the spectrum allows identifying of some very weak bands and thus two assumed combination bands at 1771 and 1871 cm^{-1} appear.

The side-on range of the (4,12) spectrum resembles the one of the (4,9) and the (4,11) spectra. In the end-on range, we observe a single strong band at 2187 cm^{-1} with a sideband at 2170 cm^{-1} to the left. There are additional weaker bands at 2215 , 2249 , 2277 , 2312 , and 2334 cm^{-1} . The latter two are accompanied by sidebands at 2317 and 2327 cm^{-1} .

The IR-PD spectra of the (4,m) cluster comprise of a multitude of bands that indicate a co-existence of side-on and end-on N_2 adsorbate molecules. Except for the IR-PD bands, which nearly match the free N_2 stretching vibration in frequency, the IR-PD adsorption bands in the end-on region show the typical red shift with respect to the free N_2 stretching vibration,⁸⁵ as also observed in our previous studies of other transition metal clusters.^{62,67–70,88,90} The total amount of IR-PD bands as compared to the total number of N_2 ligands reveals evidence for highly symmetric structures in some cases, and evidence for structural isomers in others. For the IR-PD bands in the side-on region, we observe a significant red shift of the most intense band from 1475 cm^{-1} in (4,3) to 1395 cm^{-1} in (4,12). Regarding this shift we remind the reader of our previous and detailed study on the adsorption of the initial N_2 molecules to the Ta_4^+ cluster.² There we have described and discussed an increase in the corresponding $N-N_{(\text{side-on})}$ bond distance upon coordination of a terminally coordinated N_2 molecule to an adjacent Ta atom. These previous findings up to $m = 4$ are extended up to $m = 12$ by the current experiment.

Next, we consult quantum chemical modelling results in order to enhance our understanding of the experimental IR-PD spectra of (4,m), $m = 1-12$. There are two new findings which deserve special attention.

Firstly, we address the question of why some experimental IR-PD bands in the end-on region ($2100-2400\text{ cm}^{-1}$) do not exhibit the typical and expected redshift, but most closely correspond to the frequency of free N_2 . This is remarkable, and it warrants further interpretation efforts. With the in detail discussed reaction paths of the first second and third N_2 activation from our prior publication on

the cationic Ta_4^+ cluster² at hand, we obtained a multitude of model structures with IR-PD features within the end-on region. In this context, the I1 type structures and geometry and their simulated IR-PD frequencies are of particular interest (Fig. 8, Fig. S7, Table S21). The N_2 coordinating Ta atom is crucial, and in particular its involvement into nitrido bonds (none, one, two or up to three). In consequence the red shift of IR-PD frequency diminishes with respect to free N_2 . In the Ta_4^+ cluster without any nitride ligands I1^{Ta1}_(4,1) the bond lengths $Ta-N_{(end-on)}$ and $N-N_{(end-on)}$ are 2.126 02 Å and 1.108 33 Å, respectively. The simulated and unscaled IR-PD frequency for the NN stretching vibration is 2238 cm^{-1} . In comparison to this, DFT modelling revealed for I1^{Ta4}_(4,2) a significantly longer bond $Ta-N_{(end-on)}$ of 2.285 13 Å, a correspondingly shorter bond $N-N_{(end-on)}$ of 1.098 05 Å and a higher IR-PD frequency at 2323 cm^{-1} . In this I1 type structure, the tetrahedral framework of the Ta_4^+ cluster is loaded by two nitrides on the edges opposite the Ta atom, which binds the N_2 ligands in an end-on motif. Even though the N_2 molecule adsorbs to a Ta center of the cluster which is not yet involved in a nitride bridge, the nitride ligands reveal an elongated $Ta-N_{(end-on)}$ bond, a correspondingly shorter $N-N_{(end-on)}$ bond, and an increased NN stretching frequency with respect to the cluster without nitride ligands, I1^{Ta1}_(4,1). In the case of I1^{Ta3}_(4,2), the N_2 ligand is adsorbed onto a Ta center (Ta3) that participates in a nitride bridge, correspondingly the $Ta-N_{(end-on)}$ bond is lengthened to 2.301 32 Å while the $N-N_{(end-on)}$ bond is simultaneously shortened to 1.096 18 Å. The simulated and unscaled IR-PD frequency of the NN stretching vibration accordingly blue-shifts to 2360 cm^{-1} . The N_2 adsorption to the Ta center which participates in two nitride bridges [I1^{Ta2}_(4,2)] yields an even longer $Ta-N_{(end-on)}$ bond (2.362 96 Å), an even shorter $N-N_{(end-on)}$ bond (1.091 43 Å) and even higher IR-PD frequency for the NN stretching (2431 cm^{-1}). This trend also results for I1 type structures for a Ta_4^+ cluster loaded by four nitride ligands: I1_(4,3). The IR-PD frequency of the NN stretching vibration increases from 2266 cm^{-1} via 2431 to 2472 cm^{-1} by coordination of the end-on N_2 ligand to a tantalum atom participating in only a single nitride bridge [I1^{Ta4}_(4,3)], via coordination to a tantalum atom participating in two nitride bridges [I1^{Ta1}_(4,3)], and finally to N_2 ligand coordination to a tantalum atom that is part of three nitride bridges [I1^{Ta3}_(4,3)]. Also, there is the trend of increasing bond lengths $Ta-N_{(end-on)}$ and decreasing bond lengths $N-N_{(end-on)}$ with increasing number of nitride ligands in close proximity to the Ta atom, which is the adsorption center for the end-on N_2 ligand, from 2.239 15 and 1.099 63 Å [I1^{Ta4}_(4,3) $Ta-N_{(end-on)}$ and $N-N_{(end-on)}$, respectively] to 2.357 14 and 1.090 95 Å [I1^{Ta1}_(4,3) $Ta-N_{(end-on)}$ and $N-N_{(end-on)}$, respectively] to 2.399 13 and 1.088 99 Å [I1^{Ta3}_(4,3) $Ta-N_{(end-on)}$ and $N-N_{(end-on)}$, respectively].

The above discussed trends show a correlation of N_2 bond length and N_2 coordination site with the DFT predicted NN IR-PD stretching frequency. The coordinating Ta center proves crucial: Its involvement into none, one, two or three $Ta^{(\delta+)}-N^{(\delta-)}$ bonds tunes its total partial charge and thereby its donor-acceptor capabilities. Accordingly, the coordinating intact N_2 adsorbate probes this partial charge and tells via its observable N_2 stretching mode frequency. Note, that many of the recorded IR-PD spectra reveal three sharp spectral features in the N_2 end-on stretching range.

Next, we want to address the conceivable existence of structural isomers for the various cluster adsorbate complexes. This seems nec-

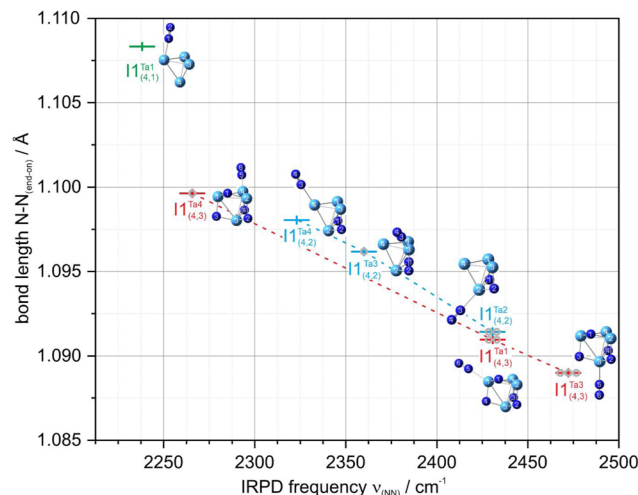


FIG. 8. Multitude of I1 type model structures and their simulated IR frequencies of the first second and third N_2 activation from our prior publication on the cationic Ta_4^+ cluster.² The N_2 coordinating Ta atom is crucial, and in particular its involvement into nitride bonds (none, one, two or up to three). In consequence the red shift of IR frequency diminishes with respect to free N_2 (2330 cm^{-1}).⁸⁵ The dotted lines serve to guide the eye. None, one, two or three open black circles at the computed data points indicate an according number of nitride bonds of the N_2 end-on coordinating Ta atom. An according trend in the $Ta-N$ bond length is found in Fig. S7 in the supplementary material.

essary in view of the many IR-PD bands that in some cases exceed the amount of adsorbed N_2 molecules. Our DFT modeling revealed such conceivable N_2 adsorption isomers, starting with the species (4,3) as dealt with in our previous study.² This species resulted from the three subsequent nitrogen adsorption, activation, and cleavage pathways in front of an unsurmountable barrier as the final product species I2_(4,3). It comprises of two fully cleaved N_2 molecules and a side-on $\mu_2-\kappa N1:\kappa N1,N2$ N_2 ligand (cf. Fig. S8, Tables S22a and S23a). The vibrational frequency for the side-on $\mu_2-\kappa N1:\kappa N1,N2$ N_2 ligand obtained from the DFT calculations was scaled to the experimentally measured IR-PD band by a scaling factor of 0.9736. This scaling factor is applied to the determined IR-PD frequencies for all further modelled species (4,m). Predicted doublet states are more stable than quartet states, and we therefore focus on the doublet ground states throughout. In order to label conceivable isomers we augment the already known nomenclature (n,m) by alphabetic indices from a – w.

There are four distinguishable Ta centers which may act as coordination sites for the adsorption of the fourth N_2 molecule to the presumed I2_(4,3) isomer. Accordingly, four structural isomers (4,4)a, (4,4)b, (4,4)c and (4,4)d result, within a total energy span of mere 4.3 kJ/mol (cf. Fig. S8, Tables S22b and S23b). From an energetic point of view, all four isomers may be populated. The scaled frequency and (4,4)c match the experimental range of observed band at 1454 cm^{-1} . Likewise, the predicted IR band of the end-on bound N_2 stretching vibration falls very well within the range of the broad experimental adsorption band around 2300 cm^{-1} .

If we take these isomers (4,4)a, (4,4)b (4,4)c and (4,4)d as starting points for the adsorption of a fifth N_2 molecule, we obtain eight isomers of the type (4,5), cf. supplementary material Fig. S9,

Tables S22c and S23c). The modelled IR spectra of (4,5)a, (4,5)d, and (4,5)f reflect quite well the experimentally measured IR-PD band at 1443 cm^{-1} and also provide three distinguishable bands in the end-on region that might well correspond to the broad experimental IR-PD adsorption band. The less stable isomer (4,5)c, $+11.0\text{ kJ/mol}$, may reflect the weak experimental sideband at 1428 cm^{-1} . This results in four isomers for species (4,5), which in turn are the starting point for the adsorption of the next (sixth) N_2 molecule.

Within an energy span of 92 kJ/mol we found in total 21 stable adsorption isomers (4,6) all of which are based on the $\text{I}_{2(4,3)}$ core structure (cf. Fig. S9, Tables S22d and S23d). We chose for further discussion seven stable isomers: (4,6)a, (4,6)c, (4,6)f, (4,6)g, (4,6)k, (4,6)l and (4,6)o. All of them derive from above discussed isomers of (4,5)a, (4,5)c, (4,5)d and (4,5)f, by addition of a single end-on coordinated N_2 . They provide for predicted IR bands that might match the observed IR-PD bands in the N_2 end-on stretching region. In total, they make up for a possible assignment of the observed experimental IR-PD pattern, cf. Fig. S9. Note, that the predicted 1663 cm^{-1} band finds no obvious counterpart in the IR-PD spectra. There are two bands close by at 1491 and 1580 cm^{-1} , but they deviate significantly. A closer look at the bond distances $d(\text{Ta4-N6})$ and angles $\angle(\text{Ta4-Ta1-N6})$ of the eight computed isomers (4,6)a, (4,6)c, (4,6)f, (4,6)g, (4,6)k, (4,6)l, (4,6)o and (4,6)r indicates increase an increasing tilt of the side-on $\mu_2\text{-}\kappa\text{N}:\kappa\text{N,N}$ N_2 ligand with the observed red shift of its IR-PD vibrational frequency (cf. Table S24). We speculate that the observed IR-PD bands at 1491 and 1580 cm^{-1} might stem from some isomers similar to (4,6)r but with slightly shorter Ta4-N6 bonds and smaller angles $\angle(\text{Ta4-Ta1-N6})$, possibly enabled by mere re-orientation of some N_2 spectator ligand, while keeping hapticity as investigated.

For species (4,7) the recorded IR-PD spectrum is particularly interesting as it shows merely two intensive bands, one in the side-on and one in the end-on range, with four very weak IR-PD bands, two in the side-on and end-on range, respectively. Speculating about a single (4,7) isomer of high symmetry, we conducted our DFT survey of conceivable structures (cf. Tables S22e and S23e) and found numerous ones, although over a wide range of relative stabilities. A mixture of seven favorable isomers – (4,7)c, (4,7)g, (4,7)l, (4,7)k, (4,7)q, (4,7)s and (4,7)t – might reproduce the measured IR-PD spectrum (cf. Fig. S10). While for species (4,6) the assignment of the calculated IR bands to the weak adsorption bands in the side-on region was difficult, for species (4,7) the isomers (4,7)l and (4,7)k reproduce the weak bands at 1478 and 1535 cm^{-1} very well. It seems, that in this case we managed to identify N_2 spectator ligand orientations that modulate the tilted N_2 stretching frequency close to observation. As a matter of fact, it is a range of computed variations in the tilting angle $\angle(\text{Ta4-Ta1-N6})$ of mere two degrees ($40^\circ\text{--}42^\circ$) and a variation of coordination distance $d(\text{Ta4-N6})$ of 0.1 \AA ($2.1\text{--}2.2\text{ \AA}$) which suffices to induce side-on N_2 stretching frequency shifts of up 145 cm^{-1} ($1404\text{--}1549\text{ cm}^{-1}$, cf. Table S24), in close correspondence to the experimental span of 113 cm^{-1} in the range of IR-PD bands ($1422\text{--}1535\text{ cm}^{-1}$). The obvious mismatch in predicted IR and observed IR-PD intensities of these bands may signify reduced rates of formation and thus reduced populations. Other than fingerprinting co-existing isomers, there is some alternative explanation for the two weak bands at 1478 and 1535 cm^{-1} in terms of combination bands. The most favorable isomer (4,7)c reveals a

bending vibration of the side-on $\mu_2\text{-}\kappa\text{N}:\kappa\text{N,N}$ N_2 ligand at 111 cm^{-1} , which simultaneously represents bond compression and elongation of the Ta4-Ta2 bond, and a wagging mode of the $\text{N}_{2(\text{end-on})}$ ligand on Ta2 at 51 cm^{-1} (cf. Table S25). These two might couple to the side-on N_2 stretching mode at 1406 cm^{-1} (calc.)/ 1422 cm^{-1} (IR-PD) and thereby explain the observed side bands.

It shows, that the according computations finds likewise numerous conceivable isomers of (4,8) (Tables S22f and S23f) as anticipated from the many observed bands, which exceed the amount of available N_2 ligands, that may act as chromophores. A selection of six isomers, (4,8)c, (4,8)e, (4,8)f, (4,8)g, (4,8)l and (4,8)q, comes close to interpret the experimental IR-PD spectrum of (4,8) (cf. Fig. S10). It seems unlikely that the significantly strong IR-PD bands at 1468 and 1564 cm^{-1} would originate from combination bands. We may note in passing that the chosen isomers derive from likely (4,7) isomers by single N_2 end-on addition to varying adsorption sites, but without further isomerization amongst the previous N_2 ligands.

Furthermore, these seven chosen (4,8) isomers serve well to generate accordingly those five favorable (4,9) isomers ((4,9)b, (4,9)d, (4,9)f, (4,9)g, (4,9)h) which might interpret major parts of the observed IR-PD spectrum (cf. Fig. S11, Tables S22g and S23g). It takes, however, some additional isomer, as e.g. (4,9)j to interpret the IR-PD band at 1399 cm^{-1} . If indeed present, it cannot originate directly from any of the six considered (4,8) isomers by mere N_2 attachment. Thus, it either stems from another, yet unknown (4,8) isomer, or it forms by N_2 attachment to some of the above listed (4,8) isomers with concomitant or subsequent but swift isomerization. The IR-PD spectrum reveals a weak adsorption at 1561 cm^{-1} indicating a side-on $\mu_2\text{-}\kappa\text{N}:\kappa\text{N,N}$ N_2 ligand with a slightly larger Ta4-N6 bond and a larger angle $\angle(\text{Ta4-Ta1-N6})$. No suitable calculated isomer has yet been found for this. It warrants to deliberate the significant splitting of the intensive end-on N_2 stretching doublet at 2215 and 2265 cm^{-1} ($\Delta\nu = 50\text{ cm}^{-1}$) and the meager splitting of the considerably strong doublet at 2327 and 2336 cm^{-1} ($\Delta\nu = 9\text{ cm}^{-1}$). The 50 cm^{-1} splitting finds interpretation through the computed (4,9)g and (4,9)h isomers, which reveal computed splittings of $\Delta\nu = 38$ and 36 cm^{-1} , respectively. These originate from symmetrically and asymmetrically coupled pairs of end-on bound N_2 oscillators that locate on neighboring Ta centers with a direct metal-to-metal bond, and without bridging nitrides or side-on coordinated N_2 in between. This situation allows for both a considerable coupling strength and high IR intensities. The latter arise from electron density shuffling across the metallic Ta-Ta bond, in phase with the N_2 stretching motion (cf. Fig. S13). The vibrational analysis of isomers (4,9)d and (4,9)j predicts symmetrically and asymmetrically coupled pairs of terminal N_2 ligands with a small splitting of $\Delta\nu = 13\text{ cm}^{-1}$, which might resemble the observed 9 cm^{-1} splitting of the two $2327\text{--}2336\text{ cm}^{-1}$ IR-PD bands. Here, the active oscillators locate on adjacent Ta centers with a direct metal-metal bond and without bridging nitrides or bridging side on coordinated N_2 ligands. Note, that two of the chosen favored isomers, (4,8)b and (4,8)f, reveal some pairs of end-on coordinated N_2 ligands with asymmetric/symmetric N_2 stretching modes that experience particularly high splittings of $\Delta\nu = 62$ and 63 cm^{-1} , respectively. The coordinating, neighboring Ta centers are bound to each other directly by a metal-to-metal bond and without bridging nitrides in between. The computed frequencies of these N_2 stretching doublet

coincide well with observed IR-PD bands in the 2200 and 2340 cm^{-1} range.

The isomer cascade of successive, stepwise N_2 adsorptions to the Ta_4^+ cluster predicts seven favorable isomers (4,10)g, (4,10)h, (4,10)j, (4,10)l, (4,10)o, (4,10)q and (4,10)r (cf. Fig. S11, Tables 22h and 23h) which altogether succeed to reproduce the observed IR-PD spectrum conclusively, but for some detail. In the side-on N_2 stretching range the following assignment can be made: isomer (4,10)q, (4,10)l and (4,10)o provides stretching modes that match the experimental IR-PD bands at 1484, 1395 and 1403 cm^{-1} . For the single band at 1423 cm^{-1} , isomer (4,10)r is found to deliver a match. Contributions from the three isomers (4,10)g, (4,10)h and (4,10)j manage to provide for a match to the broad experimental IR-PD band at 1443 and 1449 cm^{-1} . In the end-on range above 2000 cm^{-1} suitable modes of the seven selected isomers represent the recorded IR-PD bands quite well. A particular highlight is the stunning agreement of the predicted end on N_2 stretching bands of the isomers (4,10)l, (4,10)o, (4,10)q and (4,10)r with the measured IR-PD band pattern at 2300, 2313, 2319, 2328 and 2335 cm^{-1} . The observed intense N_2 stretching doublet at 2204 and 2265 cm^{-1} of (4,10) closely resembles a similar pattern in (4,9). These arise from symmetrically and asymmetrically coupled pairs of terminally bound N_2 oscillators located at neighboring Ta centers, Ta2 and Ta4, with a direct metal-metal bond and no bridging nitrides or side-on coordinated $\mu_2\text{-}\kappa\text{N}:\kappa\text{N}:\text{N}$ N_2 in between. With the adsorption cascade progressing, the number of adsorbed N_2 ligands increases stepwise, and with it the number of N_2 oscillators at the centers Ta2 and Ta4. As a consequence, the symmetric/asymmetric coupling of neighboring N_2 oscillators seems to diminish in favor of either globally coupled many oscillators or of few locally isolated N_2 stretching modes, maybe single ones. However, the adsorption band at 1561 cm^{-1} finds no counterpart in any predicted mode of any of the computed isomers. At least, our computed results for some adsorption isomers with less N_2 ligands, such as (4,7), did reveal some IR frequencies in this range with a side-on $\mu_2\text{-}\kappa\text{N}:\kappa\text{N}:\text{N}$ N_2 ligand with a slightly larger Ta4–N6 bond and a larger angle \angle (Ta4–Ta1–N6). It is well possible that our thorough survey of favorable isomers failed to achieve completeness, and we may have missed such a structural motif that likely contributes.

The recorded IR-PD bands of species (4,11) find, once more, a valid assignment by the computed predictions (cf. Fig. S12, Tables 22i and 23i): A mixture of isomers (4,11)s and (4,11)t provide for side-on coordinated N_2 oscillators that match very well the observed band at 1376 cm^{-1} , and according oscillators in isomers (4,11)a and (4,11)p resemble the intensive IR-PD band at 1395 cm^{-1} . The moderate IR-PD band at 1414 cm^{-1} and the weak IR-PD band at 1432 cm^{-1} may arise from side-on coordinated oscillators at isomers (4,11)f and (4,11)l. In the frequency range of end-on coordinated N_2 oscillators there are three intensive IR-PD bands at 2203, 2258 and 2334 cm^{-1} , which find an interpretation in terms of N_2 ligands at isomers (4,11)a, (4,11)l and (4,11)t. Further weak IR-PD bands in this range, at 2183, 2225 and 2297 cm^{-1} , may arise from isomers (4,11)f, (4,11)p and (4,11)s.

From our kinetic studies presented and discussed in the supplementary material (cf. Text S9, Fig. S24 and Table S31) we know that (4,12) is the most abundant complex at long reaction times, accompanied by a very minor (4,13) product and the smaller species (4,8), (4,9), (4,10) and (4,11) in equilibrium. Thus, (4,12)

became the largest N_2 adsorbate complex of our current IR-PD study. It finds interpretation in terms of a mixture of five favorable isomers (cf. Fig. S12, Tables 22j and 23j): (4,12)a, (4,12)d, (4,12)l, (4,12)o and (4,12)s. Two predicted IR bands from a side-on and end-on coordinated N_2 ligand each of isomer (4,12)a provide for an assignment of the intensive IR-PD bands at 1395 and 2187 cm^{-1} . Isomers (4,12)d and (4,12)o suit very well to interpret the weak IR-PD band at 1374 cm^{-1} and the IR-PD bands in the 2300 to 2340 cm^{-1} range. The moderate IR-PD band at 1417 cm^{-1} may result from isomer (4,12)i. In the five favored isomers, at least four or five of the end-on coordinated N_2 ligands are located at Ta centers Ta2 and Ta4 with a direct metal-metal bond, and no bridging nitrides or side-on coordinated N_2 in between. In the previous discussed, smaller cluster adsorbate complexes, the N_2 oscillators at these very two Ta centers provide for intense IR-PD doublets. With an increasing amount of N_2 ligands, both the IR-PD experiment and the DFT modelling of the complex (4,12) diminish the prior doublet to a single intense band at 2200 cm^{-1} , with some weak bands to the blue side, mostly beyond 2280 cm^{-1} . Upon saturation many N_2 ligands seem to experience a reduced/weak coordination to their Ta coordination sites, and accordingly a small or even vanishing redshift with respect to the stretching mode of a free N_2 molecule. In remarkable contrast, some isomers provide for a single end-on coordinated N_2 ligand that experiences a redshifted and intensively IR active stretching mode that indicates much stronger Ta– N_2 interaction.

IR-PD experiments and DFT modelling of (4,m) tantalum cluster N_2 adsorbate complexes confirms double activation and nitride formation, succeeded by single side-on N_2 coordination. Significant red shifts of IR-PD bands from these side-on coordinated $\mu_2\text{-}\kappa\text{N}:\kappa\text{N}:\text{N}$ N_2 ligands correlate with the degree of tilting towards the second coordinating Ta center. All subsequently attaching N_2 adsorbates coordinate in an end-on fashion, and we find clear evidence for co-existence of end-on coordination isomers. A large fraction, maybe the majority, of end-on coordinated N_2 ligands experience weak interaction with their coordination centers and reveal little to no red shift of their stretching frequencies, some of them even a slight blue shift. The tetrahedral Ta_4^+ framework persists but for some minor bond length relaxations.

CONCLUSION

We present an IR-PD study of selected tantalum cluster adsorbate complexes $[\text{Ta}_n(\text{N}_2)_m]^+$, abbreviated (n,m), $n = 2\text{--}4$, [IRS1]. In the adjoined IR-PD study [IRS2] we present our corresponding findings on larger complexes $[\text{Ta}_{5-8}(\text{N}_2)_m]^+$. The overall picture of N_2 adsorption onto the smallest Ta_n^+ clusters, $n = 2\text{--}4$, provides clear evidence for activation and cleavage of the initially adsorbing N_2 molecules.

We observe no structured IR-PD signal of the tantalum dimer species $[\text{Ta}_2(\text{N}_2)_1]^+$: (2,1). This primarily proves that Ta_2^+ adsorbs an N_2 molecule that is not terminally bound to the Ta_2^+ dimer in end-on coordination. Indeed, our IR-PD experiments and DFT modeling confirm and extend a previous study of Ta_2^+ clusters under ambient conditions,¹ and we identify an additional submerged entry channel barrier, such that spontaneous N_2 bond cleavage by Ta_2^+ is well confirmed.

We also present a detailed study of the N_2 adsorbate complexes of the Ta_3^+ cluster from IR-PD experiments and DFT modeling.

There is a striking absence of any vibrational bands in the IR-PD spectra of the first three adsorbate complexes (3,1), (3,2) and (3,3). In contrast, the IR-PD spectra of the species (3,4) and (3,5) do reveal some broad vibrational bands. Our DFT modelling revealed an overall exoergic reaction pathway with all submerged barriers. Initial triplet and quintet states of Ta_3^+ seem to spin quench into the singlet $^1I_{3(3,1)}$ intermediate by N_2 coordination and exoergic activation, and the reaction proceeds towards ultimate N_2 cleavage via another spin flip, likely into most stable triplet state of geminal edge-surface N–N coordination. Most noteworthy, this Ta_3^+ activation pathway proceeds much in line with our previously identified across edge above surface (AEAS) mechanism of Ta_4^+ .² This successful and simple cleavage of a first N_2 molecule by Ta_3^+ is followed by the second N_2 molecule undergoing similar activation steps until the cluster complex in $I_{3(3,2)}$ might get stuck in front of an unsurmountable barrier that hinders isothermal activation. An ultimate NN bond cleavage would be possible under adiabatic conditions. We identify an N_2 activation reaction pathway similar to the one of (2,1) for the adsorption of the third N_2 molecule on the Ta_3^+ cluster via a μ_2 - $\kappa N_5, N_6$: $\kappa N_5, N_6$ double side-on “butterfly” N_2 motif across the Ta1–Ta3 edge, yielding a single $^{1a,1b}III_{(3,3)}$ intermediate. From (3,4) on, the sequential adsorption of further N_2 molecules proceeds towards an end-on majority. The cluster adsorbate complex $^{1a,1b}III_{(3,3)}$ offers three distinguishable adsorption sites for further N_2 adsorption. The fourth, fifth and sixth N_2 molecules then coordinate on each of these free adsorption sites.

The study of the N_2 adsorbate complexes of Ta_4^+ presented here extends our earlier study and previously published spectra from (4,m), $m = 1$ –5,² up to $m = 12$. In the past study, we have investigated N_2 cleavage on the Ta_4^+ cluster surface and we discussed the underlying reaction processes. The AEAS mechanism found provided a mechanistic understanding of the light N_2 cleavage which is the basis of this current work. The present IR-PD experiments and DFT modelling of the higher loaded N_2 adsorbate species (4,m), $m > 5$, confirm the published double activation and nitride formation, succeeded by single side-on N_2 coordination. Significant red shifts of IR-PD bands from these side-on coordinated μ_2 - κN : κN , N_2 ligands correlate with the degree of tilting towards the second coordinating Ta center. All subsequently attaching N_2 adsorbates coordinate in an end-on fashion, and we find clear evidence for co-existence of end-on coordination isomers.

DFT predictions and IR fingerprints agree well in the case of Ta_4^+ , and there are no indications for dark IR bands of intact N_2 adsorbates in this case. This likely seems to hold for Ta_5^+ as well: Intact N_2 ligands yield some IR-PD bands, albeit sometimes weak ones (cf. our adjoined IR-PD study [IRS2]). A strict experimental proof would arise from future tagging experiments, or from future two color pump-probe experiments. The above findings find strong support through our complementary cryogenic kinetic studies, as documented in the supplementary material. The N_2 adsorption reaches a limit $m_{(max)}$, which depends on cluster size n . We observe a final equilibrium among those adsorbate complexes which possess up to three to five N_2 adsorbates less than $m_{(max)}$, in all cases but $n = 2$. In the cases of $n = 2$ and 3 the largest observable cluster adsorbate complex ($2, m_{(max)}$) and ($3, m_{(max)}$), respectively, are the most abundant complexes in equilibrium m^* , as well. Kinetic fits revealed significant N_2 desorption rates upon higher N_2 loads, and the vari-

ations of absolute rates find reasonable interpretation in terms of simple thermodynamic arguments. The kinetic findings provide for independent support of N_2 activation and likely cleavage.

The Ta_3^+ cluster experiences stepwise N_2 adsorption close to collision rate. There are either two dips in N_2 adsorption, at $k_{(3,2)}$ and $k_{(3,5)}$, or two spikes in N_2 desorption, at $k_{-(3,3)}$ and $k_{-(3,6)}$. Both variants find support by the IR-PD findings, and from the DFT modelling. We obtained new insights from the confirmation and extension of our prior study of N_2 activation by Ta_4^+ .² At high N_2 loads, $k_{(4,7)}$ to $k_{(4,11)}$, kinetic fits necessitate mechanisms beyond stepwise N_2 adsorption/desorption, such as e.g. adsorption isomers - and/or adsorbate shell reordering. Such a hypothesis is also well in line with the IR-PD findings and the DFT modelling.

We strongly encourage future experiments on a direct spectral identification and characterization of tantalum nitride bonds through their IR fingerprints, e.g. by application of far IR radiation from a free electron laser source.

SUPPLEMENTARY MATERIAL

Supplementary material comprises of comprehensive listings of energetics, structures and IR frequencies of computed structures, of plots energetics of reaction pathways by other multiplicities, of further computed IR spectra, and of multiple text blocks and viewgraphs on the conducted kinetic experiments, kinetic fits and their interpretation in detail.

ACKNOWLEDGMENTS

This work was supported by the German research foundation DFG within the trans-regional collaborative research center SFB/TRR 88 (Cooperative effects in homo and heterometallic complexes, 3met.de) and by the research center OPTIMAS. We thank Thomas Kolling for technical assistance and valuable discussion. Quantum chemical modelling took place at the “Regionales Hochschulrechenzentrum Kaiserslautern” (RHRK).

AUTHOR DECLARATIONS

Conflict of Interest

The authors have no conflicts to disclose.

Author Contributions

The experiments were performed by DVF with MPK, AS and MEH, and DVF performed the quantum chemical calculations. ML and CW assisted on experiments and calculations. The evaluation of the measured data was carried out by DVF, and it was accompanied by discussions with AS, MPK and GNS. DVF and GNS wrote the manuscript, which all of the authors revised and agreed to.

Daniela V. Fries: Data curation (lead); Formal analysis (equal); Investigation (lead); Project administration (equal); Validation (equal); Writing – original draft (equal); Writing – review & editing (equal). **Matthias P. Klein:** Conceptualization (supporting);

Data curation (supporting); Formal analysis (supporting); Investigation (supporting); Methodology (equal); Validation (supporting); Writing – review & editing (supporting). **Annika Straßner**: Data curation (supporting); Formal analysis (supporting); Investigation (supporting); Methodology (supporting); Validation (supporting); Writing – review & editing (supporting). **Maximilian E. Huber**: Data curation (supporting); Formal analysis (supporting); Investigation (supporting); Project administration (supporting); Validation (supporting); Writing – review & editing (supporting). **Maximilian Luczak**: Data curation (supporting); Formal analysis (supporting); Investigation (supporting); Methodology (supporting); Software (supporting); Validation (supporting); Writing – review & editing (supporting). **Christopher Wiehn**: Data curation (supporting); Formal analysis (supporting); Investigation (supporting); Methodology (supporting); Software (supporting); Validation (supporting); Writing – review & editing (supporting). **Gereon Niedner-Schatteburg**: Conceptualization (lead); Funding acquisition (lead); Methodology (lead); Project administration (lead); Resources (lead); Supervision (lead); Writing – original draft (equal); Writing – review & editing (equal).

DATA AVAILABILITY

The data that support the findings of this study are available from the corresponding author upon reasonable request.

REFERENCES

- C. Geng, J. Li, T. Weiske, and H. Schwarz, *Proc. Natl. Acad. Sci. U. S. A.* **115**(46), 11680–11687 (2018).
- D. V. Fries, M. P. Klein, A. Steiner, M. H. Prosenc, and G. Niedner-Schatteburg, *Phys. Chem. Chem. Phys.* **23**(19), 11345–11354 (2021).
- X. Zhang, B. B. Ward, and D. M. Sigman, *Chem. Rev.* **120**(17), 9834 (2020).
- X. Zhang, B. B. Ward, and D. M. Sigman, *Chem. Rev.* **120**(12), 5308–5351 (2020).
- D. E. Canfield, A. N. Glazer, and P. G. Falkowski, *Science* **330**(6001), 192–196 (2010).
- H. Liu, *Ammonia Synthesis Catalysts* (World Scientific, Singapore, 2013).
- R. Schlögl, *Ammonia Synthesis in Handbook of Heterogeneous Catalysis* (Wiley VCH, 2008).
- M. Appl, *Ammonia: Principles and Industrial Practice* (Wiley VCH, 2007).
- G. Ertl, *Angew. Chem., Int. Ed.* **47**(19), 3524–3535 (2008).
- G. Ertl, S. B. Lee, and M. Weiss, *Surf. Sci.* **114**(2-3), 515–526 (1982).
- G. Ertl, *Catal. Rev.* **21**(2), 201–223 (1980).
- R. Schlögl, *Angew. Chem., Int. Ed.* **42**(18), 2004–2008 (2003).
- H. Liu, *Chin. J. Catal.* **35**(10), 1619–1640 (2014).
- H.-P. Jia and E. A. Quadrelli, *Chem. Soc. Rev.* **43**(2), 547–564 (2014).
- S. J. K. Forrest, B. Schluschaß, E. Y. Yuzik-Klimova, and S. Schneider, *Chem. Rev.* **121**(11), 6522–6587 (2021).
- S. Kim, F. Loose, and P. J. Chirik, *Chem. Rev.* **120**(12), 5637–5681 (2020).
- R. J. Burford and M. D. Fryzuk, *Nat. Rev. Chem.* **1**(4), 0026 (2017).
- P. Avenier, M. Taoufik, A. Lesage, X. Solans-Monfort, A. Baudouin, A. de Mallmann, L. Veyre, J.-M. Basset, O. Eisenstein, L. Emsley, and E. A. Quadrelli, *Science* **317**(5841), 1056–1060 (2007).
- J. Li and S. Li, *Angew. Chem., Int. Ed.* **47**(42), 8040–8043 (2008).
- R. A. J. O’Hair and G. N. Khairallah, *J. Cluster Sci.* **15**(3), 331–363 (2004).
- D. K. Böhme and H. Schwarz, *Angew. Chem., Int. Ed.* **44**(16), 2336–2354 (2005).
- P. B. Armentrout, *Catal. Sci. Technol.* **4**(9), 2741–2755 (2014).
- M. Zhou, X. Jin, Y. Gong, and J. Li, *Angew. Chem., Int. Ed.* **46**(16), 2911–2914 (2007).
- X. Cheng, Z.-Y. Li, L.-H. Mou, Y. Ren, Q.-Y. Liu, X.-L. Ding, and S.-G. He, *Chem. - Eur. J.* **25**(72), 16523–16527 (2019).
- Y. Gong, Zhao, and M. Zhou, *J. Phys. Chem. A* **111**(28), 6204–6207 (2007).
- L.-H. Mou, Y. Li, G.-P. Wei, Z.-Y. Li, Q.-Y. Liu, H. Chen, and S.-G. He, *Chem. Sci.* **13**(32), 9366–9372 (2022).
- Z.-Y. Li, Y. Li, L.-H. Mou, J.-J. Chen, Q.-Y. Liu, S.-G. He, and H. Chen, *J. Am. Chem. Soc.* **142**(24), 10747–10754 (2020).
- L.-H. Mou, Y. Li, Z.-Y. Li, Q.-Y. Liu, H. Chen, and S.-G. He, *J. Am. Chem. Soc.* **143**(45), 19224–19231 (2021).
- Z.-Y. Li, F. Horn, Y. Li, L.-H. Mou, W. Schöllkopf, H. Chen, S.-G. He, and K. R. Asmis, *Chem. - Eur. J.* **29**(14), e202203384 (2022).
- Y.-Q. Ding, Z.-Y. Chen, Z.-Y. Li, X. Cheng, M. Wang, and J.-B. Ma, *J. Phys. Chem. A* **126**(9), 1511–1517 (2022).
- J. F. Eckhard, D. Neuwirth, C. Panosetti, H. Oberhofer, K. Reuter, M. Tschurl, and U. Heiz, *Phys. Chem. Chem. Phys.* **19**(8), 5985–5993 (2017).
- N. Levin, J. T. Margraf, J. Lengyel, K. Reuter, M. Tschurl, and U. Heiz, *Phys. Chem. Chem. Phys.* **24**(4), 2623–2629 (2022).
- M. R. Zakin, D. M. Cox, and A. Kaldor, *J. Chem. Phys.* **87**(8), 5046–5048 (1987).
- J. F. Eckhard, T. Masubuchi, M. Tschurl, R. N. Barnett, U. Landman, and U. Heiz, *J. Phys. Chem. A* **125**(24), 5289–5302 (2021).
- J. F. Eckhard, T. Masubuchi, M. Tschurl, R. N. Barnett, U. Landman, and U. Heiz, *J. Phys. Chem. C* **122**(44), 25628–25637 (2018).
- C. Geng, J. Li, T. Weiske, and H. Schwarz, *Proc. Natl. Acad. Sci. U. S. A.* **116**(43), 21416–21420 (2019).
- X. Sun and X. Huang, *ACS Omega* **7**(26), 22682–22688 (2022).
- G.-D. Jiang, L.-H. Mou, J.-J. Chen, Z.-Y. Li, and S.-G. He, *J. Phys. Chem. A* **124**(38), 7749–7755 (2020).
- M. Kumar Yadav and A. Mookerjee, *Physica B* **405**(18), 3940–3942 (2010).
- F. Mafuné, Y. Tawaraya, and S. Kudoh, *J. Phys. Chem. A* **120**(24), 4089–4095 (2016).
- M. C. Tsai, U. Ship, I. C. Bassignana, J. Küppers, and G. Ertl, *Surf. Sci.* **155**(2-3), 387–399 (1985).
- H. J. Freund, B. Bartos, R. P. Messmer, H. Grunze, H. Kühlenbeck, and M. Neumann, *Surf. Sci.* **185**(1-2), 187–202 (1987).
- P. Maitre, D. Scuderi, D. Corinti, B. Chiavarino, M. E. Crestoni, and S. Fornarini, *Chem. Rev.* **120**(7), 3261–3295 (2020).
- J. R. Eyler, *Mass Spectrom. Rev.* **28**(3), 448–467 (2009).
- J. Oomens, B. G. Sartakov, G. Meijer, and G. von Helden, *Int. J. Mass Spectrom.* **254**(1-2), 1–19 (2006).
- A. Fielicke, A. Kirilyuk, C. Ratsch, J. Behler, M. Scheffler, G. Von Helden, and G. Meijer, *Phys. Rev. Lett.* **93**(2), 023401 (2004).
- J. Roithová, *Chem. Soc. Rev.* **41**(2), 547–559 (2012).
- G. Altinay and R. B. Metz, *Int. J. Mass Spectrom.* **297**(1-3), 41–45 (2010).
- B. Chiavarino, M. E. Crestoni, M. Schütz, A. Bouchet, S. Piccirillo, V. Steinmetz, O. Dopfer, and S. Fornarini, *J. Phys. Chem. A* **118**(34), 7130–7138 (2014).
- O. Dopfer, *J. Phys. Org. Chem.* **19**(8-9), 540–551 (2006).
- N. I. Hammer, J. W. Shin, J. M. Headrick, E. G. Diken, J. R. Roscioli, G. H. Weddle, and M. A. Johnson, *Science* **306**(5696), 675–679 (2004).
- J. M. Headrick, E. G. Diken, R. S. Walters, N. I. Hammer, R. A. Christie, J. Cui, E. M. Myshakin, M. A. Duncan, M. A. Johnson, and K. D. Jordan, *Science* **308**(5729), 1765–1769 (2005).
- A. M. Rijs and J. Oomens, *Top. Curr. Chem.* **364**, 1–42 (2015).
- T. R. Rizzo and O. V. Boyarkin, *Top. Curr. Chem.* **364**, 43–98 (2015).
- T. R. Rizzo, J. A. Stearns, and O. V. Boyarkin, *Int. Rev. Phys. Chem.* **28**(3), 481–515 (2009).
- W. H. Robertson and M. A. Johnson, *Annu. Rev. Phys. Chem.* **54**, 173–213 (2003).
- D. Schröder, S. Shaik, and H. Schwarz, *Acc. Chem. Res.* **33**(3), 139–145 (2000).
- H. Schwarz, *Catal. Sci. Technol.* **7**(19), 4302–4314 (2017).
- P. Gruene, A. Fielicke, and G. Meijer, *J. Chem. Phys.* **127**(23), 234307 (2007).
- J. Du, X. Sun, and G. Jiang, *J. Chem. Phys.* **136**(9), 094311 (2012).
- L.-H. Mou, Z.-Y. Li, and S.-G. He, *J. Phys. Chem. Lett.* **13**(18), 4159–4169 (2022).

- ⁶²J. Mohrbach, S. Dillinger, and G. Niedner-Schatteburg, *J. Phys. Chem. C* **121**(20), 10907–10918 (2017).
- ⁶³S. Dillinger, J. Mohrbach, and G. Niedner-Schatteburg, *J. Chem. Phys.* **147**(18), 184305 (2017).
- ⁶⁴A. A. Ehrhard, M. P. Klein, J. Mohrbach, S. Dillinger, and G. Niedner-Schatteburg, *Mol. Phys.* **119**(17–18), e1953172 (2021).
- ⁶⁵A. A. Ehrhard, M. P. Klein, J. Mohrbach, S. Dillinger, and G. Niedner-Schatteburg, *J. Chem. Phys.* **156**(5), 054308 (2022).
- ⁶⁶A. Straßner, M. P. Klein, D. V. Fries, C. Wiehn, M. E. Huber, J. Mohrbach, S. Dillinger, D. Spelsberg, P. B. Armentrout, and G. Niedner-Schatteburg, *J. Chem. Phys.* **155**(24), 244306 (2021).
- ⁶⁷A. Straßner, C. Wiehn, M. P. Klein, D. V. Fries, S. Dillinger, J. Mohrbach, M. H. Prosen, P. B. Armentrout, and G. Niedner-Schatteburg, *J. Chem. Phys.* **155**(24), 244305 (2021).
- ⁶⁸S. Dillinger, J. Mohrbach, J. Hewer, M. Gaffga, and G. Niedner-Schatteburg, *Phys. Chem. Chem. Phys.* **17**(16), 10358–10362 (2015).
- ⁶⁹S. Dillinger, M. P. Klein, A. Steiner, D. C. McDonald, M. A. Duncan, M. M. Kappes, and G. Niedner-Schatteburg, *J. Phys. Chem. Lett.* **9**(4), 914–918 (2018).
- ⁷⁰M. P. Klein, A. A. Ehrhard, J. Mohrbach, S. Dillinger, and G. Niedner-Schatteburg, *Top. Catal.* **61**(1–2), 106–118 (2018).
- ⁷¹M. J. Frisch, G. W. Trucks, H. B. Schlegel, G. E. Scuseria, M. A. Robb, J. R. Cheeseman, G. Scalmani, V. Barone, B. Mennucci, G. A. Petersson, H. Nakatsuji, M. Caricato, X. Li, H. P. Hratchian, A. F. Izmaylov, J. Bloino, G. Zheng, J. L. Sonnenberg, M. Hada, M. Ehara, K. Toyota, R. Fukuda, J. Hasegawa, M. Ishida, T. Nakajima, Y. Honda, O. Kitao, H. Nakai, T. Vreven, J. A. Montgomery, Jr., J. E. Peralta, F. Ogliaro, M. Bearpark, J. J. Heyd, E. Brothers, K. N. Kudin, V. N. Staroverov, R. Kobayashi, J. Normand, K. Raghavachari, A. Rendell, J. C. Burant, S. S. Iyengar, J. Tomasi, M. Cossi, N. Rega, J. M. Millam, M. Klene, J. E. Knox, J. B. Cross, V. Bakken, C. Adamo, J. Jaramillo, R. Gomperts, R. E. Stratmann, O. Yazyev, A. J. Austin, R. Cammi, C. Pomelli, J. W. Ochterski, R. L. Martin, K. Morokuma, V. G. Zakrzewski, G. A. Voth, P. Salvador, J. J. Dannenberg, S. Dapprich, A. D. Daniels, Ö. Farkas, J. B. Foresman, J. V. Ortiz, J. Cioslowski, and D. J. Fox, *GAUSSIAN 09, Revision E.01*, Gaussian, Inc., Wallingford, CT, 2009.
- ⁷²M. J. Frisch, G. W. Trucks, H. B. Schlegel, G. E. Scuseria, M. A. Robb, J. R. Cheeseman, G. Scalmani, V. Barone, G. A. Petersson, H. Nakatsuji, X. Li, M. Caricato, A. V. Marenich, J. Bloino, B. G. Janesko, R. Gomperts, B. Mennucci, H. Hratchian, J. V. Ortiz, A. F. Izmaylov, J. L. Sonnenberg, D. Williams-Young, F. Ding, F. Lipparini, F. Egidi, J. Goings, B. Peng, A. Petrone, T. Henderson, D. Ranasinghe, V. G. Zakrzewski, J. Gao, N. Rega, G. Zheng, W. Liang, M. Hada, M. Ehara, K. Toyota, R. Fukuda, J. Hasegawa, M. Ishida, T. Nakajima, Y. Honda, O. Kitao, H. Nakai, T. Vreven, K. Throssell, J. A. Montgomery, Jr., J. E. Peralta, F. Ogliaro, M. J. Bearpark, J. J. Heyd, E. N. Brothers, K. N. Kudin, V. N. Staroverov, T. A. Keith, R. Kobayashi, J. Normand, K. Raghavachari, A. P. Rendell, J. C. Burant, S. S. Iyengar, J. Tomasi, M. Cossi, J. M. Millam, M. Klene, C. Adamo, R. Cammi, J. W. Ochterski, R. L. Martin, K. Morokuma, O. Farkas, J. B. Foresman, and D. J. Fox, *GAUSSIAN 16, Revision C.01*, Gaussian, Inc., Wallingford, CT, 2016.
- ⁷³J. P. Perdew, K. Burke, and M. Ernzerhof, *Phys. Rev. Lett.* **78**(7), 1396 (1997).
- ⁷⁴C. Adamo and V. Barone, *J. Chem. Phys.* **110**(13), 6158–6170 (1999).
- ⁷⁵F. Weigend and R. Ahlrichs, *Phys. Chem. Chem. Phys.* **7**(18), 3297–3305 (2005).
- ⁷⁶D. Andrae, U. Häußermann, M. Dolg, H. Stoll, and H. Preuß, *Theor. Chim. Acta* **77**(2), 123–141 (1990).
- ⁷⁷D. Figgen, K. A. Peterson, M. Dolg, and H. Stoll, *J. Chem. Phys.* **130**(16), 164108 (2009).
- ⁷⁸J. Mohrbach, S. Dillinger, and G. Niedner-Schatteburg, *J. Chem. Phys.* **147**(18), 184304 (2017).
- ⁷⁹H. B. Schlegel, *J. Comput. Chem.* **3**(2), 214–218 (1982).
- ⁸⁰C. Peng and H. Bernhard Schlegel, *Isr. J. Chem.* **33**(4), 449–454 (1993).
- ⁸¹H. P. Hratchian and H. B. Schlegel, *Theory and Applications of Computational Chemistry*, edited by C. E. Dykstra, G. Frenking, K. S. Kim, and G. E. Scuseria (Elsevier, Amsterdam, 2005), pp. 195–249.
- ⁸²K. Fukui, *Acc. Chem. Res.* **14**(12), 363–368 (1981).
- ⁸³C. Lee, W. Yang, and R. G. Parr, *Phys. Rev. B* **37**(2), 785–789 (1988).
- ⁸⁴A. D. Becke, *J. Chem. Phys.* **98**(7), 5648–5652 (1993).
- ⁸⁵W. M. Haynes, *CRC Handbook of Chemistry and Physics* (CRC Press Taylor & Francis Group, 2014).
- ⁸⁶G. Blyholder, *J. Phys. Chem.* **68**(10), 2772–2777 (1964).
- ⁸⁷J. Chatt and L. A. Duncanson, *J. Chem. Soc.* **1953**, 2939–2947.
- ⁸⁸M. P. Klein, A. A. Ehrhard, M. E. Huber, A. Straßner, D. V. Fries, S. Dillinger, J. Mohrbach, and G. Niedner-Schatteburg, *J. Chem. Phys.* **156**(1), 014302 (2022).
- ⁸⁹M. P. Klein, Doctoral thesis, Technische Universität Kaiserslautern, 2021.
- ⁹⁰S. Dillinger, Doctoral thesis, Technische Universität Kaiserslautern, 2017.